**Prediction and control of symmetry breaking in embryoid bodies by environment and signal integration**

Naor Sagy, Shaked Slovin, Maya Allalouf, Maayan Pour, Gaya Savyon, Jonathan Boxman, Iftach Nachman*

Department of Biochemistry and Molecular Biology, Tel Aviv University, Israel

Correspondence to IN: iftachn@tauex.tau.ac.il

**Abstract**

During early embryogenesis, mechanical constraints and localized biochemical signals co-occur around anteroposterior axis determination and symmetry breaking. Their relative roles, however, are hard to tease apart in vivo. Using Brachyury (Bra), a primitive streak and mesendoderm marker in EBs, we study how contact, biochemical and neighboring cell cues affect the positioning of a primitive streak-like locus, determining the AP axis. We show that a Bra-competent layer must be formed in the EB before Bra expression initiates, and that Bra onset locus position is biased by contact points of the EB with its surrounding, likely through chemical cues modulation rather than by mechanical signaling. We can push or pull Bra onset away from contact points by introducing a separate localized Wnt signal source, maneuver Bra onset to a few loci, or to an isotropic peripheral pattern. Finally, we show Foxa2+ cells are predictive of the future location of Bra onset, demonstrating an earlier symmetry-breaking event. Our analysis of factors affecting symmetry breaking and spatial fate choice during this developmental process may prove valuable for in vitro differentiation and organoid formation.

**Introduction**

In the early mouse embryo, the blastocyst implants into the uterus wall on the fourth day of gestation. A series of events follows, among which is the formation of an anteroposterior (AP) axis, initiated by the localization of anterior visceral endoderm (AVE) cells at the prospective anterior side and emergence of the primitive streak (PS) at the posterior side (Arnold and Robertson, 2009). The PS is formed through interaction between BMP, Nodal, FGF and Wnt pathways at the posterior side of the blastocyst, and limited to that side by inhibitory signals originating from the AVE at the anterior side (Arnold and Robertson, 2009; Robertson, 2005). Mechanical pressure, presumably stemming from the uterus wall, was suggested to be necessary for proper AP axis formation, including the positioning of the AVE and elongation of the egg cylinder (Hiramatsu et al., 2013), though this dependence was later challenged (Bedzhov et al., 2015). Mechanical strain associated with gastrulation was also demonstrated to drive mesoderm specification in fish, fly and sea anemones through modification of beta-catenin (Brunet et al., 2013; Pukhlyakova et al., 2018). Another factor shaping PS and AP axis formation is the visceral endoderm layer, characterized at E5.5 by the expression of Foxa2. As mechanical signals, localized biochemical signals and neighboring cell layer contexts all co-occur in a specific reproducible pattern during embryogenesis, it is very hard to dissect their respective roles and dependencies in specifying PS location selection and axis formation.

In-vitro multi-cellular models such as embryoid bodies (EBs), and gastruloids derived from EBs, have been used in recent years to dissect certain aspects of early embryonic development (Poh et al., 2014; Turner et al., 2014; van den Brink et al., 2014; Warmflash et al., 2014). These models are formed by 3D aggregation of pluripotent stem cells. Given proper conditions, these aggregates will differentiate in a partially organized manner, break their radial symmetry and develop an AP axis (Beccari et al., 2018; ten Berge et al., 2008; van den Brink et al., 2014). Interestingly, when aggregated from a small number of cells and under specific signal conditions, EBs form "gastruloids", displaying not only initial symmetry breaking but multiple axes as well as elongation (Turner et al., 2017; van den Brink et al., 2014). Germ layer structure was also shown in confined 2D colonies (Etoc et al., 2016; Morgani et al., 2018; Warmflash et al., 2014). More recently, it was shown that by mixing mouse ES cells with extra-embryonic cells it is possible to obtain in vitro structures that resemble early stage mouse embryos, both by gene expression profile and morphologically, including dual axis formation (Harrison et al., 2017; Sozen et al., 2018). The success of these in-vitro structures in capturing some of the spatiotemporal aspects of early embryogenesis make them valuable model systems for studying basic principles of early development, in addition to strategies of in vitro differentiation and tissue engineering. One of the earliest fate decisions that can be observed in embryonic stem cells is their differentiation to mesendoderm progenitors, which are characteristic of the PS and are marked by Brachyury (Gadue et al., 2006; Kubo et al., 2004; Tada et al., 2005). In 2D patterned colonies, the biased onset pattern of Bra has been associated with colony geometry as well as cell density (Blin et al., 2018). In 3D models such as EBs and gastruloids, the polar onset pattern of Bra expression provides one of the first detectable events of symmetry breaking (Beccari et al., 2018; Blin et al., 2018; Boxman et al., 2016; ten Berge et al., 2008; van den Brink et al., 2014). The mechanisms leading to the spatial selection of this pole and axis formation in these 3D models are, however, not clear.

Here we show that Bra expression onset is influenced by contact in EBs. While the entire EB outer shell has the potential to express Bra, the expression of this regulator is initiated at the EB contact point with its surrounding surface. By manipulating the EB's environment we were able to alter the onset of Bra expression to either multiple loci, to a wide contact surface or to an isotropic pattern throughout the outer shell. By creating spatially separate sources of contact and biochemical signals, we demonstrate how the tissue can integrate these two modalities to define a single Bra locus. Remarkably, Foxa2 appears with an eccentric bias towards the future onset site of Bra, evident of an earlier symmetry breaking event, and revealing different dependencies on Wnt signaling.

Our findings provide insight into symmetry breaking mechanisms in 3D tissue models, and primitive streak spatial selection *in utero*, demonstrating how contact and biochemical signals may integrate to drive symmetry breaking and mesendoderm differentiation.

## Results

### Brachyury expression onset location in embryoid bodies is influenced by contact

We have previously observed that in EBs differentiated within agarose microwells in the absence of strong Wnt activation, Bra expression predominantly starts from a single locus on the EB external shell, and spreads in that layer towards the opposite pole, where a locus is defined as a cluster of Bra+ cells (see Methods) (Boxman et al., 2016). However, it is unclear whether the spatial selection of the locus is an outcome of stochastic symmetry breaking within the EB, and why Bra onsets solely on the outer shell and not in the volume. Mouse Brachyury-GFP E14 ES cells (Fehling et al., 2003) pre-grown in serum-LIF conditions were suspended in differentiation medium, aggregated into EBs in hanging drops for 24 hours and then seeded in agarose microwell arrays for live imaging up to Brachyury-GFP onset (~72 hrs), or differentiated within the hanging drops for a similar period (Fig. 1A). We find that in EBs differentiated in agarose microwells, Bra expression onsets from the EB's contact point with the microwell's wall or floor (Fig. 1B-F, Movie S1-S4). Out of 47 successfully imaged EBs, 16 showed Bra onset at the bottom, 12 showed side onset, 14 showed joint side and bottom onset (Fig. 1C) and 5 showed two disparate onset loci. We noted that side-onset or dual-onset EBs are generally larger than bottom onset ones (mean EB radius=120um, σ=16um, vs. mean radius=95um, σ=17um, P=0.001), raising the hypothesis that side onset is driven by contact with the side wall, which is more common in larger EBs. This is reinforced by examining EBs with two Bra loci, which we found to be touching the microwell boundaries at two points or a large surface area overlapping the onset loci (Fig. 1D). We therefore compared in a separate experiment the onset angles in bottom-only contact EBs (n=9) with EBs touching the side wall (n=10), finding significant difference indicating that indeed onset location is affected by contact (Fig. 1F, p=3e-5, two-sample Kolmogorov-Smirnov (KS) test). Interestingly, EBs differentiated in hanging drops also display a single locus Bra pattern (Fig. 2B). Since EBs grown in hanging drops lie at the drop's bottom boundary, we hypothesized their onset may also be biased toward this boundary. The alternative result would be random spatial onset, either due to lack of an organizing event or due to random rotations of the EB in the drop. Analyzing the locus location in hanging drops (n=12, p-value=1e-5, KS test), we indeed find that Bra locus onsets from the bottom, similarly to the bottom-contact EBs grown in microwells (Fig. 1F). Taken together, we find both mechanical contact and confinement by liquid to air interface can determine the onset location of Bra in EBs. Such contact dependence may be explained by signal consolidation around the contact interface and/or by mechano-sensing pathways.

We next wanted to check whether the timing and location of Bra onset can be controlled by imposing contact at a specific locus at an early stage. To this end, we fabricated 200um wide rectangular “micropool” structures to enforce early contact at two sides of the EB (Fig. 1G,H). Out of the EBs grown in these micropools, 30/41 touched the micropool walls and 11/41 contacted only the well bottom. In the side-contacting group, 29/30 expressed Bra at their side-contact points, compared to 2/11 non-touching EBs with side onset (p-value<1e-5, Fisher's exact test, Movie S5, S6). Out of the side-contact, side-onset EBs, 26/29 showed a single locus onset (Fig. 1G), 3/29 showed simultaneous onset at two loci (Fig. 1H). The preference of one side may result from earlier Bra triggering on that side due to faster signal consolidation, allowing enough time for the signal to spread towards the other side and mask or prevent the formation of a second locus. EBs grown in wider micropools (500um

width) and which did not touch the walls showed bottom Bra expression onset, at the contact point with the plate floor (8/10), similar to the case in large microwells (n>50 in multiple experiments [20]). We then evaluated the effect of early contact on the timing of Bra onset. When grown in the narrow (200um) micropools, EBs created contact with the micropool sides earlier (50-60 hours), but Bra onset did not occur earlier compared to the non-touching controls in the wide micropools (79h, σ=2 hrs, n=11 vs. 75h, σ=5 hrs, n=5). This suggests that cells on the outer shell of the EB did not yet have the potential to express Bra when contact was initially applied to the EB, and more molecular changes had to take place before Bra onset could occur around the contact point.

**Brachyury competent shell is formed prior to onset**

The observation that EBs can form multiple contact loci or an entire cap contact locus when confined in micropools raised the question whether the potential to express Bra is limited to specific areas on the outer layer of the EB, to the entire shell, or is uniform throughout the EB volume. Growing EBs in hanging drops, we first confirmed that a canonical Wnt activation reporter (SuTOP-CFP, (Serup et al., 2012)) showed co-localization with Bra, in agreement with observations that Bra is activated via the canonical Wnt pathway (Fig. S1A) (Arnold et al., 2000; ten Berge et al., 2008). We then tested EB spatial limitations for Bra onset under external Wnt induction. To this end, we induced the canonical Wnt pathway by either adding CHIR99021 (CHIR), a small-molecule Wnt pathway agonist bypassing the pathway receptor via Gsk3β inhibition, by adding soluble Wnt3a ligand, or by embedding Wnt3a-coated beads within the entire EB volume during aggregation (Fig. S1B) (Habib et al., 2013). EBs under CHIR treatment showed isotropic onset, with no distinct locus, suggesting that the entire outer shell is Bra competent (n=16/16, Fig. 2B, center). Activation by soluble Wnt3a resulted in a stronger, yet polarized locus (n=10/10, Fig. 2B, right) (ten Berge et al., 2008). EBs embedded with Wnt3a beads from aggregation displayed isotropic or near isotropic Bra expression onset on the outer shell at 72 hours, similar to CHIR treated EBs, which can be attributed to multiple loci caused by different beads (Fig. S1C). As in our forced early contact results, Wnt3a beads did not lead to Bra expression up until 72hrs after aggregating the EBs, nor did they induce Bra under pluripotency conditions (Fig. S1B, left). These results confirm that similar to their susceptibility to contact, outer-layer cells need to reach a certain maturation stage before becoming Wnt-susceptible to activate Brachyury.

As the entire outer shell is Bra-competent, and as contact is associated with Bra onset locus, we hypothesized that given uniform contact conditions, outer layer cells may induce Bra in a spherically isotropic pattern. We therefore tested the Bra onset pattern when EBs were differentiated while embedded in rich ECM composition (Matrigel) or in a more biologically-inert hydrogel (low gelling point agarose). When embedded in Matrigel, EBs in a range of sizes displayed isotropic onset pattern (13/15, mean radius at onset=95um, σ=50um), while two large EBs (r=120um, 180um) initiated Bra from a distinct locus (Fig. 2C, Movie S7, S8). To test whether the effect of Matrigel was mainly due to mechanical pressure or due to biochemical interactions with its components, we tested the dynamics when embedded in low melting point agarose of lower (0.5%), similar (1%) or higher (1.5%) stiffness compared to Matrigel. When embedded in agarose, the EBs generated a single locus onset despite having an isotropic contact with the gel (0.5%, n=14/14; 1%, n=10/10; 1.5%, n=11/12; Fig. 2D). When differentiating uniformly small EBs in microwells (mean EB radius at onset=78um, σ=10um, n=9), Bra-GFP showed a uniform isotropic onset (7/8 EBs, average onset time 78h, σ=9h), similar to small EBs embedded in Matrigel (Fig. S1D). This suggests an isotropic

pattern can be a result of size, which may be explained by a minimal locus size that is larger than the small EB surface, or a minimal signal gradient requirement for a polarized pattern. In summary, given sufficient EB size, a polarized Bra pattern can be obtained at contact points, but also under uniform gel contact, suggesting this is a robust EB behavior. However, as our results from CHIR induction, Wnt3a bead embedding and growth in Matrigel demonstrate, the entire outer shell is competent to activate Bra, given strong activation of the Wnt pathway.

Previously, Oct4 and Sox2 expression levels in differentiating ES cells were suggested to direct their differentiation toward mesendoderm or neural ectoderm, respectively (Thomson et al., 2011). To test whether the competence of the outer shell can be explained by the expression pattern of these early pluripotency factors, we immunostained for Oct4 and Sox2 at 17, 48, 76 and 111 hrs into differentiation. We indeed observed that the expression of both genes recedes from the center towards the outer shell with time, and by 72 hrs both Sox2 and Oct4 are highly expressed only at the outer shell of the EB (Fig. 2E).

Which molecular components may mediate the effect of contact on Bra onset in outer layer cells? Previously, fibronectin was shown to induce Bra expression, and a mechanism linking fibronectin to Wnt signaling was proposed (Cheng et al., 2013). We therefore hypothesized such a link can explain both the relation between contact and Wnt signaling (leading to Bra onset), and the location choice for the Bra locus. We found fibronectin is expressed isotropically on the EB's outer shell, implying that its mere expression does not determine the location of Bra onset (Fig. 3A). We then inhibited fibronectin activity using an anti-Fn1 antibody, starting from 0, 24, 48, or 72 hours following aggregation under differentiation conditions. Compared to the control group, which displayed normal Bra expression (16/16), fibronectin inhibition added at aggregation or at 24hr inhibited Bra expression (10/10 and 6/6 EBs, respectively, $p<2e-5$), had little to no effect when added at 72hr (4/4 EBs, $p<3e-4$) and a mixed effect when added at 48hr (8/8 EBs, $p<2e-6$) (Fig. 3B). Lack of Bra expression under Fn1 inhibition was confirmed at the mRNA level as well (Fig. 3C). Our results suggest that the dependence of Bra positive fate on fibronectin is limited to early stages, while the accumulation of Brachyury in the cells, as well as the expansion of its expression to neighboring cells do not depend on fibronectin.

**Wnt and contact signal sources are integrated to activate Bra**

We found that both Wnt signaling and surface contact affect Bra expression onset, though our results suggest that contact bias may be mediated through biochemical signaling. To further investigate how these two signal sources relate to each other in this context, we designed a system where we create a spatial separation between surface contact point and a local source of Wnt signaling. To this end, we transfected HEK cells with a plasmid constitutively expressing either Wnt3a-P2A-H2B-CFP, Dkk1-P2A-H2B-Venus or, for the control group, H2B-CFP (Fig. 4A). A clump of HEK cells was then integrated into each EB at a random location shortly after aggregation. The EBs were then differentiated, as in the wild-type experiments, and the location of Bra locus was analyzed with respect to the contact point and the locus of signaling cells using two-photon microscopy (Fig. 4B, C, D). In the EBs containing Dkk1 or Wnt3a cell clumps, the Brachyury locus overlapped with the plane defined by EB centroid, HEKs, and contact point (n=16; average deviation from co-planarity 9.3 degrees) (Fig. S2A), which allowed us to analyze the joint effects of contact and

Wnt3a/Dkk1 signaling on Bra expression locus as angular deviations on a single plane (Fig. 4B). The amount of Wnt3a secreting agents determined the effect on Bra locus bias from the contact. For small clumps of Wnt3a expressing cells (3-5 cells), the source of Wnt3a leads to a shift in the Bra locus, so that it is positioned between the contact point and the Wnt3a expressing locus (Fig. 4C, E-G). For larger clumps of Wnt3a secreting cells (>10 cells), the Bra locus was pulled closer to the HEKs cluster, maintaining a single locus (Fig. 4E, F, $p<0.05$ for all group pairs, KS-test). In one example, where the EB touched the microwell wall at the side opposite to the HEK clump, two Bra loci emerged, one next to the HEKs and one at the side contact point (Fig. S2B). In contrast, a source of Dkk1 shifts Bra locus away from the contact point (Fig 4D, E, G, $p<0.05$ for all group pairs, KS-test). This indicates that Dkk1 can exert its limiting effect over at least 150um. Moreover, the locus shift from the contact point, towards or away from the signaling source shows how Wnt3a and Dkk1 signal integration determines the locus location. In control EBs (harboring clumps of H2B-CFP cells) we see no spatial effect on the locus of Bra onset, which is mostly at the contact point (3/4). These results suggest that contact and Wnt effects on Bra onset are integrated rather than override each other. One possible explanation is that contact mediates Wnt signaling (which then gets spatially summed with the other source of Wnt signal). It is also possible, however, that contact acts through a different signaling pathway, which gets summed with the Wnt pathway in triggering Bra onset.

**Foxa2 is a precursor to symmetry breaking and Bra onset locus**

To explain the choice of Bra onset location in the absence of external contact surfaces (i.e. in hanging drops), we examined additional genes that are predicted to be expressed at or near the primitive streak before gastrulation. We have previously suggested that once Brachyury onsets, the EB progresses at a common developmental pace, delineating a differentiation plan associated with multiple early development genes (Boxman et al., 2016). We therefore hypothesized that the spatial expression pattern of key proteins in EBs before and during Bra onset will show similarity to their *in utero* pattern around the primitive streak. To test this, we immunostained EBs differentiated in hanging drops for a few early markers at different time points from aggregation, and checked how their spatial expression patterns relate to that of Bra. We find that Eomes, a primitive streak marker regulated by Nodal and an EMT driver, was localized to the same pole as Bra though expanding further on the outer shell (Fig. 5A). E-cadherin was expressed throughout the EB prior to Bra expression onset, and then its expression declined where Bra was expressed, indicating that epithelial mesenchymal transition takes place in the EB (Fig. 5B)(ten Berge et al., 2008). Loss of E-cadherin enables cell movement, which is supportive of previous observations of gastrulation-like events in EBs and 2D models (Boxman et al., 2016; van den Brink et al., 2014; Warmflash et al., 2014), and is consistent with primitive streak behavior. Oct4, whose expression initially declines in the inner layers, is gradually receding on the outer shell towards the opposite pole as Bra expression expands, similar to the opposing gradients observed in late streak stage epiblast (Fig. 2E, 5C).

The examples above demonstrate how the expression and spatial arrangement of different proteins in the EB during pre-streak through streak phases resemble the equivalent in vivo stages, albeit with an altered topology. Since in the embryo the primitive streak is initiated adjacent to the visceral endoderm layer, we tested for spatio-temporal correlation of Foxa2, a visceral endoderm marker, with Bra in the EB. Such a correlation could point to an additional driving factor in Bra locus determination. Indeed, Foxa2 expression appeared up

to 24 hours prior to Bra at an internal area within the EBs, with Bra onset following on the shell juxtaposed to Foxa2 expressing cells (Fig. 6A), suggesting a common driver or inter-layer dependency. This spatial relation between Foxa2 and Bra is accentuated in large EBs (~700uM in diameter at onset) (Fig. 6A, bottom, Fig. S3A), and suggests these two cell populations have a regulatory relation. To better characterize Foxa2 cells around their onset, we examined the expression of Gata6 and Sox17 at 48 hrs. Sox17 was not expressed at this early time point. Similarly, no Gata6 expression was detected in the EBs (Fig S4D), consistent with previous reports (Turner et al., 2017; van den Brink et al., 2014). This indicates that Foxa2+ cells at this stage do not represent primitive endoderm or visceral endoderm, but likely posterior epiblast or early anterior streak identities (Arnold et al., 2000; Burtscher and Lickert, 2009; Cai et al., 2008; Choi et al., 2012).

To look for candidate genes that may convey the regulation of Bra next to Foxa2+ cells, we analyzed a published single cell expression dataset from E6.5 mouse embryos (Scialdone et al., 2016). We found that within epiblast cells, both Foxa2 expressing cells and Bra expressing cells are significantly enriched for Porcupine (Porcn) expression (p=2.6e-8 and p=8.83e-10, respectively). Porcupine palmitoylation of Wnt ligands is required for their secretion, suggesting that Foxa2 positive cells in EBs may secrete Wnt ligands to the adjacent perimeter, thus promoting the onset of Bra in an adjacent locus. We therefore immunostained for Porcn in differentiating EBs, finding that porcupine expression is spatially limited to areas adjacent to and overlapping Bra onset (Fig. 6B). Inhibiting Porcn activity with IWP-2 starting either at aggregation or 48hr after aggregation (when Foxa2 is already expressed in the volume) resulted in the abolishment of both Bra and Foxa2 (Fig. 6C; Fig. S4A). A similar result was obtained when selectively activating non-canonical Wnt with Wnt5a, while blocking canonical Wnt using XAV-939 or Wnt secretion using IWP-2, resulting in no expression of Bra nor Foxa2. Adding just Wnt5a had no significant effect on expression of Bra and Foxa2 when comparing to the control group. (XAV-939+Wnt5a: 0/10, p=1.2e-4; IWP-2+Wnt5a: 0/10, p=1.2e-4; Wnt5a: 8/8; Control: 6/6; Fig. S4C). This suggests that both genes require canonical Wnt signaling for their expression (Gadue et al., 2006; Sawada et al., 2005). When introducing IWP-2 with CHIR to the EBs 48hr after aggregation, we were able to rescue Bra, however Foxa2 was fully downregulated. When Wnt3a was added to IWP-2 we obtained a partial rescue of both Bra and Foxa2. Interestingly, when perturbing the EBs with just CHIR or Wnt3a, we obtained a similar result where Bra is over-expressed and Foxa2 is either fully (in the case of CHIR) or partially downregulated and spatially decoupled from Bra (in the case of Wnt3a) (Fig. 6C, D, Fig. S3B). These results suggest that an intricate, likely dynamic, signaling balance involving canonical Wnt determines and maintains the fate of these cells. In small EBs (<65um radius) Foxa2 had small to negligible expression while Bra encompassed the entire EB (5/5, Fig. S4B). This suggests that the EB requires a certain volume (or length scale) to allow the development of two distinct cell populations, consistent with results in 2D colonies (Morgani et al., 2018; Warmflash et al., 2014). The threshold size may be required to establish sufficient differences, or gradients, in signaling activity. Finally, while Bra expression was abolished under fibronectin inhibition starting at aggregation, Foxa2 showed wild type expression, pointing to a fate decision made at least 24 hours before Bra onset and leading to Foxa2+ cells (Fig. 6C, bottom).

Together these results show how Bra and Foxa2 are spatially related under canonical Wnt signaling. Bra is monotonically upregulated by canonical Wnt where Foxa2 shows a more complex regulation nature, where it is upregulated by an intermediate level but downregulated by a strong level of canonical Wnt activation (Fig. 6E).

## Discussion

Here we dissect the factors and mechanisms affecting the polarized expression pattern of Brachyury expression in embryoid bodies. These patterns can be formed in EBs and gastruloids with no extra-embryonic tissue and no external Nodal or BMP sources (Boxman et al., 2016; Turner et al., 2017; van den Brink et al., 2014). We show that physical contact with surfaces, a localized source of Wnt signaling, and proximity to Foxa2-expressing cells may all induce or predict the onset of Brachyury. Interestingly, in the embryo, these three conditions co-occur near the future location of the primitive streak, making it hard to dissect their respective roles. Brachyury onsets during gastrulation near a source of Wnt signaling (arising from a positive feedback loop between Bmp4 sourced from the ExE and Nodal and Wnt at the posterior epiblast), adjacent to Foxa2-positive cells, in a region that may experience high mechanical pressure due to implantation. Here we analyze some of the hierarchy between these three PS predictors (Fig. 6E).

Brachyury onset polarization is robust to different external conditions and EB parameters, suggesting it is the "default" behavior in this system. A similar result was demonstrated in mouse embryos grown in-vitro, where while mechanical contact may direct AP axis formation and positioning of the AVE, these can also robustly form in hanging drops (Bedzhov et al., 2015; Hiramatsu et al., 2013). The polar pattern in EBs can be obtained even in the absence of any chemical or physical cue directing its orientation (as we see in the agarose embedding experiments). Overriding this polarization process pattern in EBs requires specific intervention, such as continuous canonical Wnt activation by CHIR or applying inducing sources (contact points or localized Wnt sources) at two distant locations on the EB surface (Fig. 1G, Fig. S2B). Contact with external surfaces, or with the hanging drop boundary surface, is sufficient to bias the location of Bra onset and orient the EB primary axis. We show how through controlled contact we can generate two Bra loci, depending on the geometry of the surrounding surfaces. The fact that Bra onsets in hanging drops or large wells similarly to the way it does in narrow micropools, suggests it is not the effect of mechanical pressure, but rather the interface with contact surface or geometrical confinement. These could act through limiting the diffusion of secreted signal molecules, such as Wnt ligands, resulting in locally higher signal concentration (Siggia and Warmflash, 2018). Another option is bypassing the ligand activation mechanism through interfacing with outside surfaces by integrin-mediated signaling (Cheng et al., 2013), or by mechano-transduced phosphorylation of beta-catenin (Brunet et al., 2013), although the localization of Bra locus in hanging drops to the bottom air-liquid interface suggests that diffusion confinement may be sufficient. Interestingly, the factors we find to affect Bra locus in 3D are very different from the case of 2D patterned colonies, where a recent study related the percentage of Bra+ cells to cell density, and their localization to high curvature regions at the tip of elongated colonies (Blin et al., 2018). In 2D colonies there is no equivalent for limited ligand diffusion in 3D near surfaces, and alternative factors may bias the response potential in different locations within the colony (Etoc et al., 2016).

We find that the potential to initiate Brachyury is limited, at least in large enough EBs, to cells at the outer layers of the EB, and its expression does not expand much inwards. Whole-volume Bra expression is observed mostly in small EBs. The patterns of Sox2 and Oct4 expression suggest there may be multiple expression and epigenetic differences between different EB layers prior to Bra onset, which could explain the biased expansion pattern, despite positive feedback between Bra and Wnt signaling (Evans et al., 2012; Yamaguchi et

al., 1999). The limitation of Foxa2 initiation to inner EB cells provides further support for the differential potentials in different EB layers.

We find that we can “pull” or “push” the Bra locus away from the contact point using an external source of Wnt3a or Dkk1 secreting cells, respectively. This demonstrates that contact and biochemical signal modalities can be summed by the EB, resulting in a single locus, as opposed to the two loci, or one locus overriding the other we observe in the forced contact experiments. This can be attributed to the gradient strength or to the surface distance between the loci, which may be too large for signal integration to have an effect. One possible mechanism for this integration can be activation of Wnt signaling through the mechanical contact. The dependence of Bra activation on fibronectin may point to such a mechanism (Cheng et al., 2013). Interestingly, the mechanism proposed by Cheng et al. (2013) bypasses the Wnt pathway receptors, and therefore cannot explain why Dkk1 diverts Bra onset away from the contact point, suggesting other mechanisms may be at play. Another option is that Wnt ligands consolidate at the contact surfaces, or have limited diffusion range near them, leading to locally higher concentration (Siggia and Warmflash, 2018). This option is particularly reinforced by the localization of Bra locus to the air-water interface in hanging drops, where we do not expect to find integrin interactions. The isotropic peripheral onset we observe in small size EBs may be attributed to a lack of Wnt gradient formation.

The relation of Bra onset to Foxa2 positive cells provides some interesting insights. First, from the differential response to fibronectin inhibition, we conclude that the decision junction of differentiating ES cells within the EB toward Bra and Foxa2 tissue layers takes place at 24-48h prior to Bra onset. The lack of overlap with visceral or definitive endoderm markers suggests Foxa2+ cells initially represent a non-endodermal population, such as anterior primitive streak (Burtscher and Lickert, 2009; Gadue et al., 2006). Second, the observation that small-size EBs do not express Foxa2 suggests that a signal gradient may be controlling the segregation between these two cell populations, that potentially represent posterior and anterior primitive streak. This is reinforced by the dependency of Foxa2 expression on intermediate canonical Wnt signaling, as well as by the high spatial dependency we see between these two cell populations in large EBs (Fig. 6, S3). The fact that different perturbations can lead to Bra or Foxa2 expression while abolishing the other fate in the EB, and that the spatial adjacency of these two cell populations can be decoupled using external Wnt signaling, suggests the observed spatial relation may be due to both proteins depending on different levels of canonical Wnt signaling, that can be spatially coupled through a morphogen gradient. The earlier onset of Foxa2 relative to Bra may result from the fact that Foxa2-competent cells, which form within the inner EB layers, require lower levels of canonical Wnt (which may be reached earlier), while Bra requires higher level of canonical Wnt. Another option is that the Foxa2 locus (or its relevant enhancer) becomes accessible earlier than that of Bra. Further molecular work is needed to decipher the Foxa2 onset mechanisms.

In contrast to its location, the timing of Bra expression onset in EBs is not affected by external or localized Wnt3a signaling, or by inducing early contact in narrow microwells. These results point to the maturation needed in outer shell cells before they become Wnt and/or contact-responsive to induce Bra. Further characterization of the chromatin or expression changes defining that “mature” state are needed.

Through different perturbations on a 3D in vitro system we were able to delineate basic dependencies of an early fate decision on contact and biochemical factors that co-occur in the embryo. The insights we gained here improve our understanding on the forces shaping differentiation within in vitro systems such as EBs and gastruloids, and shed more light on how they are integrated in vivo.

## Methods

### Cell culture

E14 Bra-GFP mouse ESCs (kindly provided by Dr. Gordon Keller), R1 mouse ESCs and SuTOP-CFP,AR8-RFP mouse ESCs (kindly provided by Dr. Palle Serup) were cultured on gelatin surface using standard conditions on irradiated primary mouse embryonic fibroblasts and knockout DMEM containing 15% fetal bovine serum, 50 ug/ml penicillin/streptomycin, 2 mM L Glutamine, 100 µM non-essential amino acids, 80 µM ß-mercaptoethanol and $10^3$ U/mL LIF.

### EB formation and differentiation

Embryoid bodies were formed in hanging drops under differentiation conditions. Each drop contained 25ul differentiation medium (IMEM containing 20% FBS, 50 ug/ml penicillin/streptomycin, 2 mM L Glutamine, 100 µM non-essential amino acids, 100 µM ß-mercaptoethanol) with approximately 300 mES cells (100 cells for small EB experiments, 2000 cells for large EB experiments). Number of cells in hanging drops was controlled using a cell counting slide and then dilution of the cells-containing medium to obtain the desired starting cell number per single EB within each 25ul hanging drop. Cells were aggregated for 24\48 hours before being transferred to micropools/ microwells for imaging in the same medium. Alternatively, the EBs were kept in hanging drops for the entire duration of experiment before being imaged or fixed and immunostained. In some of the staining experiments (Fig. 3, Fig. 6A, Fig. S3), R1 derived EBs were used. In these EBs, Bra onset typically occurs about 12 hrs later than in E14 derived EBs. When adding inhibitors or activators to hanging drops we aggregated the EBs in 20ul hanging drops and then added at the appropriate time 5ul of medium with the required substance. For signal perturbation experiments, differentiation medium was supplemented with CHIR99021 (5.35 uM) or recombinant Wnt3a (500 ng/ml). For fibronectin inhibition, the medium was supplemented with anti-Fn1 antibody (Abcam ab6328). For incorporating Wnt3a-bound beads within the EB, prepared beads (kindly provided by Shukri Habib) were pre-mixed with mES cells before distributing the suspension to 25ul hanging drops for aggregation. We added 12K beads to 10ml of medium with the mES cells, averaging at 30 beads per EB. Beads integration into the EBs was confirmed by two-photon microscopy (Fig. S1B).

### Hydrogel and Matrigel

Low melting point agarose (Sigma A9414) was mixed with pre heated DDW and vortexed to avoid clumps. It was then deposited on a glass bottom of a 24-well, to allow two photon imaging, and EBs were injected into the gel when it cooled down sufficiently, about 24 hours after aggregation in hanging drops. Matrigel (Gibco Geltrex A1413202) was thawed on ice in 4 degrees overnight. Matrigel drops (20ul each) were deposited on the glass bottom of a 24-

well. The EBs were transferred into the drops at 48h after aggregation, and after gel solidification the wells were filled with differentiation medium.

**HEK incorporation in EBs**

HEK 293 cells were split to three 12-wells (50% confluence). 12 hours later, the wells were transfected with constitutive pCMV-H2B-Cerulean, pCMV-Wnt3A-P2A-H2B-Cerulean or pCMV-DKK1-P2A-H2BVenus plasmids, using the Xfect™ transfection reagent (Cat.# 631318). 24 hours post transfection, the transfected HEKs were trypsinized, suspended as single cells and injected into hanging drops containing 12-hour old E14 Bra-GFP EBs at different concentrations – 10/20/50 HEKs per EB. 24 hours later, the injected EBs were transferred into microwells and imaged using a two-photon microscope.

**Micropools patterning with Deep Reactive-Ion Etching (DRIE) and microwells**

To create the silicon template for the shaped micropools and microwells we have implemented a high aspect ratio etching system usually used for microelectronics fabrication. With DRIE we were able to determine the micro pattern's exact depth by selecting a wafer with a specific handle/ device thickness. This suggests an advantage over the common photoresist techniques, which requires fine-tuning of the process to have an exact pattern depth. We have fabricated 200-500um diameter microwells and 100-500um wide micropools, with a depth of approximately 400um. The patterns were then coated with PTFE to minimize friction with the template when pulling the elastomer out. To create the microwell/pool negative, PDMS elastomer (Sylgard 184) mixed with a curing agent (1:10) was poured into the silicon wafer mold and incubated o/n at 50C. Individual stamps were then cut out using a scalpel. To generate the positive agar microwells/pools we placed the stamps face down inside poly-D-Lysine coated glass bottom plates and injected agarose under the stamps. The plates with the injected stamps were then placed in a vacuum chamber for 90 minutes, followed by another round of agar injection and additional 10 minutes in the vacuum chamber. The stamps were then removed, leaving the micro patterns imprinted in the agar.

**Hanging drops imaging**

EBs were aggregated in hanging drops on plastics slides. The slides were mounted in the two-photon microscope and imaged with EC Plan-Neofluar 20x/0.50 dry objective, providing a working distance of 2mm. The data was then segmented in Imaris and analyzed in MATLAB.

**Live imaging**

We have sourced data from both 2D and 3D live imaging experiments. 2D epi-fluorescence experiments offer a short acquisition cycle for a large cohort of EBs, thus yielding accurate temporal tracking and statistics based on a large number of samples. On the other hand they do not possess elevation distinction and the superior resolution and cell separation that more advanced microscopy techniques offer. For 3D imaging we used a two-photon microscope with which we were able to have a full view of the signal's dynamics and track

individual cells. However, this technique requires large data analysis, had a longer acquisition cycle, and is less compatible with multiple EB imaging. Two-photon imaging was done using a Zeiss LSM7 inverted two-photon microscope with a Plan-Apochromat 20X/0.8 dry objective. Each EB was scanned at 3um intervals along the *z* direction. Horizontal resolution was set to 512x512 pixels at approximately 0.6um per pixel, 8 bit depth. GFP was excited at 930nm. RFP, Alexa 488, Alexa 405 and Alexa 594 were excited at 800nm. CFP was excited at 860 nm. Epifluorescence imaging was done using a Nikon TiE epi-fluorescence microscope equipped with a motorized XY stage (Prior) at 10x magnification using NIS Elements software. Acquisitions were taken every 25/30 minutes for 14-72 hours. For live imaging, in both systems we used Okolab incubation cages, maintaining 5% CO2 and 37C.

**RT PCR**

Three different primer pairs were designed for different Brachyury exons, and two for each of the house keeping genes Ywhaz and Rock2. EBs were gathered from different pools, distinct from each other by experiment group. mRNA was extracted by disassembling by pipetting and incubating the pooled EBs for 5 minutes in 0.5ml Trizol (Sigma Aldrich T9424-25ML), followed by adding 100ul chloroform and another 5 minutes incubation. After centrifuging the samples for 10min at 12KG, 2-8C the translucent phase was incubated in IPA 100% for 10 minutes at RT. Centrifuging the samples again at the same manner, resulted at a pellet containing the mRNA to which we added 100ul 70% ethanol, vortexed the samples and then centrifuged the samples for 5 minutes at 10KG, 2-8C. The ethanol was then removed, and the rest vaporized within 15min, followed by adding DDW. We then produced cDNA (Invitrogen 18080-051) and performed RT-PCR (Thermo Fisher StepOnePlus Real-Time PCR system) using Fast SYBR Green (Thermo-Fisher, 4385612). Each Bra primer pair was run in duplicate. Results were normalized by subtracting housekeeping genes average result ($\Delta$Ct), and then subtracting the control group (-$\Delta\Delta$Ct).

**Immunofluorescence**

We fixed the embryoid bodies with 4% Paraformaldehyde o/n at 4C, followed by rinse cycle and an o/n wash in PBS. We add primary antibody (Eomes: Abcam ab23345; Bra: R&D Systems AF2085 ; Foxa2: Abcam ab108422-100 ; E-cadherin: Cell Signaling 24E10 ; Oct4: Santa Cruz sc-8628 ; Sox2: Santa Cruz sc-365964) with blocking buffer (PBS, 0.1% Triton x100, 5% FBS) and incubate o/n at 4C, followed by four wash cycles in blocking buffer for at least half an hour per cycle. We then add the Alexa Fluor-conjugated secondary antibody in blocking buffer and incubate it o/n, followed by four wash cycle as described for the primary antibody. Antibodies concentrations used are the same as recommended by the manufacturer for 2D staining.

**Segmentation and Analysis**

The Two-photon microscopy data was contrast enhanced in Fiji and then spot segmented in Imaris, where the integration radius was set to 7um and the filter was set to sum intensity with a threshold of 110/255. The background is subtracted prior to segmentation. The segmented data was read and analyzed in MATLAB. For Bra locus estimation in hanging drops or microwell experiments, locus elevation and azimuth angles were calculated from the segmented two-photon data by the sum vector of all Bra+ cells. Bra onset was defined as “polarized” when Bra-GFP occupied less than 25% of the shell, in one locus. The EB center

and radius were estimated by Bra+ cells curvature. The angle between the EB bottom point and Bra locus was then computed. For the HEKs incorporation experiments, we developed a Matlab script that calculates geometrical properties between HEKs cluster, Bra locus and contact point. The script detects HEK cells in each time point by channel and intensity. We then calculate the geometrical mean of the HEKs and set it as the HEKs location point. Next we look for Bra locus, where a locus is defined as a minimum of 5 cells above intensity threshold of 100 within a distance of 50um from each other, all in the green channel. Next we define the contact point of the EB with the well bottom as the bottom point of the sphere and calculate the geometric properties between all pairwise combinations of HEKs cluster, Bra locus, and contact point. The geometrical properties calculated are the spatial angles, Euclidean distances and geodesic distances. Side onset in microwells was manually detected by super imposing GFP signal on brightfield images, in which both the EB and the microwell wall are clearly visible, as shown in Figure 1. Angle quantification was automatically performed using a MATLAB script on 3D segmented data.

**Acknowledgements**

We thank Shukri Habib for providing Wnt3a coated beads, Palle Serup for the SuTOP-CFP mES cell line, Amitai Menuchin for help with RT-PCR, and David Sprinzak, Omri Wurzel and the three anonymous reviewers for providing helpful feedback on the manuscript. This study was supported by the Israel Science Foundation (grant No. 1665/16) and by a fellowship from the Edmond J. Safra Center for Bioinformatics at Tel-Aviv University.

**Competing Interests**

The authors declare no competing financial interests.

**References**


Arnold, S.J., and Robertson, E.J. (2009). Making a commitment: cell lineage allocation and axis patterning in the early mouse embryo. Nature reviews Molecular cell biology *10*, 91-103.

Arnold, S.J., Stappert, J., Bauer, A., Kispert, A., Herrmann, B.G., and Kemler, R. (2000). Brachyury is a target gene of the Wnt/beta-catenin signaling pathway. Mech Dev *91*, 249-258.

Beccari, L., Moris, N., Girgin, M., Turner, D.A., Baillie-Johnson, P., Cossy, A.C., Lutolf, M.P., Duboule, D., and Arias, A.M. (2018). Multi-axial self-organization properties of mouse embryonic stem cells into gastruloids. Nature *562*, 272-276.

Bedzhov, I., Bialecka, M., Zielinska, A., Kosalka, J., Antonica, F., Thompson, A.J., Franze, K., and Zernicka-Goetz, M. (2015). Development of the anterior-posterior axis is a self-organizing process in the absence of maternal cues in the mouse embryo. Cell Res *25*, 1368-1371.

Blin, G., Wisniewski, D., Picart, C., Thery, M., Puceat, M., and Lowell, S. (2018). Geometrical confinement controls the asymmetric patterning of brachyury in cultures of pluripotent cells. Development *145*.

Boxman, J., Sagy, N., Achanta, S., Vadigepalli, R., and Nachman, I. (2016). Integrated live imaging and molecular profiling of embryoid bodies reveals a synchronized progression of early differentiation. Sci Rep *6*, 31623.

Brunet, T., Bouclet, A., Ahmadi, P., Mitrossilis, D., Driquez, B., Brunet, A.C., Henry, L., Serman, F., Bealle, G., Menager, C.*, et al.* (2013). Evolutionary conservation of early mesoderm specification by mechanotransduction in Bilateria. Nat Commun *4*, 2821.

Burtscher, I., and Lickert, H. (2009). Foxa2 regulates polarity and epithelialization in the endoderm germ layer of the mouse embryo. Development *136*, 1029-1038.

Cai, K.Q., Capo-Chichi, C.D., Rula, M.E., Yang, D.H., and Xu, X.X. (2008). Dynamic GATA6 expression in primitive endoderm formation and maturation in early mouse embryogenesis. Dev Dyn *237*, 2820-2829.

Cheng, P., Andersen, P., Hassel, D., Kaynak, B.L., Limphong, P., Juergensen, L., Kwon, C., and Srivastava, D. (2013). Fibronectin mediates mesendodermal cell fate decisions. Development *140*, 2587-2596.

Choi, E., Kraus, M.R., Lemaire, L.A., Yoshimoto, M., Vemula, S., Potter, L.A., Manduchi, E., Stoeckert, C.J., Jr., Grapin-Botton, A., and Magnuson, M.A. (2012). Dual lineage-specific expression of Sox17 during mouse embryogenesis. Stem Cells *30*, 2297-2308.

Etoc, F., Metzger, J., Ruzo, A., Kirst, C., Yoney, A., Ozair, M.Z., Brivanlou, A.H., and Siggia, E.D. (2016). A Balance between Secreted Inhibitors and Edge Sensing Controls Gastruloid Self-Organization. Dev Cell *39*, 302-315.

Evans, A.L., Faial, T., Gilchrist, M.J., Down, T., Vallier, L., Pedersen, R.A., Wardle, F.C., and Smith, J.C. (2012). Genomic targets of Brachyury (T) in differentiating mouse embryonic stem cells. PloS one *7*, e33346.

Fehling, H.J., Lacaud, G., Kubo, A., Kennedy, M., Robertson, S., Keller, G., and Kouskoff, V. (2003). Tracking mesoderm induction and its specification to the hemangioblast during embryonic stem cell differentiation. Development *130*, 4217-4227.

Gadue, P., Huber, T.L., Paddison, P.J., and Keller, G.M. (2006). Wnt and TGF-beta signaling are required for the induction of an in vitro model of primitive streak formation using embryonic stem cells. Proceedings of the National Academy of Sciences of the United States of America *103*, 16806-16811.
Habib, S.J., Chen, B.C., Tsai, F.C., Anastassiadis, K., Meyer, T., Betzig, E., and Nusse, R. (2013). A localized Wnt signal orients asymmetric stem cell division in vitro. Science *339*, 1445-1448.
Harrison, S.E., Sozen, B., Christodoulou, N., Kyprianou, C., and Zernicka-Goetz, M. (2017). Assembly of embryonic and extraembryonic stem cells to mimic embryogenesis in vitro. Science *356*.
Hiramatsu, R., Matsuoka, T., Kimura-Yoshida, C., Han, S.W., Mochida, K., Adachi, T., Takayama, S., and Matsuo, I. (2013). External mechanical cues trigger the establishment of the anterior-posterior axis in early mouse embryos. Dev Cell *27*, 131-144.
Kubo, A., Shinozaki, K., Shannon, J.M., Kouskoff, V., Kennedy, M., Woo, S., Fehling, H.J., and Keller, G. (2004). Development of definitive endoderm from embryonic stem cells in culture. Development *131*, 1651-1662.
Morgani, S.M., Metzger, J.J., Nichols, J., Siggia, E.D., and Hadjantonakis, A.K. (2018). Micropattern differentiation of mouse pluripotent stem cells recapitulates embryo regionalized cell fate patterning. Elife *7*.
Poh, Y.C., Chen, J., Hong, Y., Yi, H., Zhang, S., Chen, J., Wu, D.C., Wang, L., Jia, Q., Singh, R.*, et al.* (2014). Generation of organized germ layers from a single mouse embryonic stem cell. Nat Commun *5*, 4000.
Pukhlyakova, E., Aman, A.J., Elsayad, K., and Technau, U. (2018). beta-Catenin-dependent mechanotransduction dates back to the common ancestor of Cnidaria and Bilateria. Proceedings of the National Academy of Sciences of the United States of America *115*, 6231-6236.
Robertson, E.J. (2005). Making heads and tails of the early mouse embryo. Harvey Lect *101*, 59-73.
Sawada, A., Nishizaki, Y., Sato, H., Yada, Y., Nakayama, R., Yamamoto, S., Nishioka, N., Kondoh, H., and Sasaki, H. (2005). Tead proteins activate the Foxa2 enhancer in the node in cooperation with a second factor. Development *132*, 4719-4729.
Scialdone, A., Tanaka, Y., Jawaid, W., Moignard, V., Wilson, N.K., Macaulay, I.C., Marioni, J.C., and Gottgens, B. (2016). Resolving early mesoderm diversification through single-cell expression profiling. Nature *535*, 289-293.
Serup, P., Gustavsen, C., Klein, T., Potter, L.A., Lin, R., Mullapudi, N., Wandzioch, E., Hines, A., Davis, A., Bruun, C.*, et al.* (2012). Partial promoter substitutions generating transcriptional sentinels of diverse signaling pathways in embryonic stem cells and mice. Disease models & mechanisms *5*, 956-966.
Siggia, E.D., and Warmflash, A. (2018). Modeling Mammalian Gastrulation With Embryonic Stem Cells. Curr Top Dev Biol *129*, 1-23.
Sozen, B., Amadei, G., Cox, A., Wang, R., Na, E., Czukiewska, S., Chappell, L., Voet, T., Michel, G., Jing, N.*, et al.* (2018). Self-assembly of embryonic and two extra-embryonic stem cell types into gastrulating embryo-like structures. Nat Cell Biol *20*, 979-989.
Tada, S., Era, T., Furusawa, C., Sakurai, H., Nishikawa, S., Kinoshita, M., Nakao, K., Chiba, T., and Nishikawa, S. (2005). Characterization of mesendoderm: a diverging point of the definitive endoderm and mesoderm in embryonic stem cell differentiation culture. Development *132*, 4363-4374.

ten Berge, D., Koole, W., Fuerer, C., Fish, M., Eroglu, E., and Nusse, R. (2008). Wnt signaling mediates self-organization and axis formation in embryoid bodies. Cell stem cell *3*, 508-518.
Thomson, M., Liu, S.J., Zou, L.N., Smith, Z., Meissner, A., and Ramanathan, S. (2011). Pluripotency factors in embryonic stem cells regulate differentiation into germ layers. Cell *145*, 875-889.
Turner, D.A., Girgin, M., Alonso-Crisostomo, L., Trivedi, V., Baillie-Johnson, P., Glodowski, C.R., Hayward, P.C., Collignon, J., Gustavsen, C., Serup, P., *et al.* (2017). Anteroposterior polarity and elongation in the absence of extra-embryonic tissues and of spatially localised signalling in gastruloids: mammalian embryonic organoids. Development *144*, 3894-3906.
Turner, D.A., Rue, P., Mackenzie, J.P., Davies, E., and Martinez Arias, A. (2014). Brachyury cooperates with Wnt/beta-catenin signalling to elicit primitive-streak-like behaviour in differentiating mouse embryonic stem cells. BMC biology *12*, 63.
van den Brink, S.C., Baillie-Johnson, P., Balayo, T., Hadjantonakis, A.K., Nowotschin, S., Turner, D.A., and Martinez Arias, A. (2014). Symmetry breaking, germ layer specification and axial organisation in aggregates of mouse embryonic stem cells. Development *141*, 4231-4242.
Warmflash, A., Sorre, B., Etoc, F., Siggia, E.D., and Brivanlou, A.H. (2014). A method to recapitulate early embryonic spatial patterning in human embryonic stem cells. Nature methods *11*, 847-854.
Yamaguchi, T.P., Takada, S., Yoshikawa, Y., Wu, N., and McMahon, A.P. (1999). T (Brachyury) is a direct target of Wnt3a during paraxial mesoderm specification. Genes Dev *13*, 3185-3190.

**Figures**

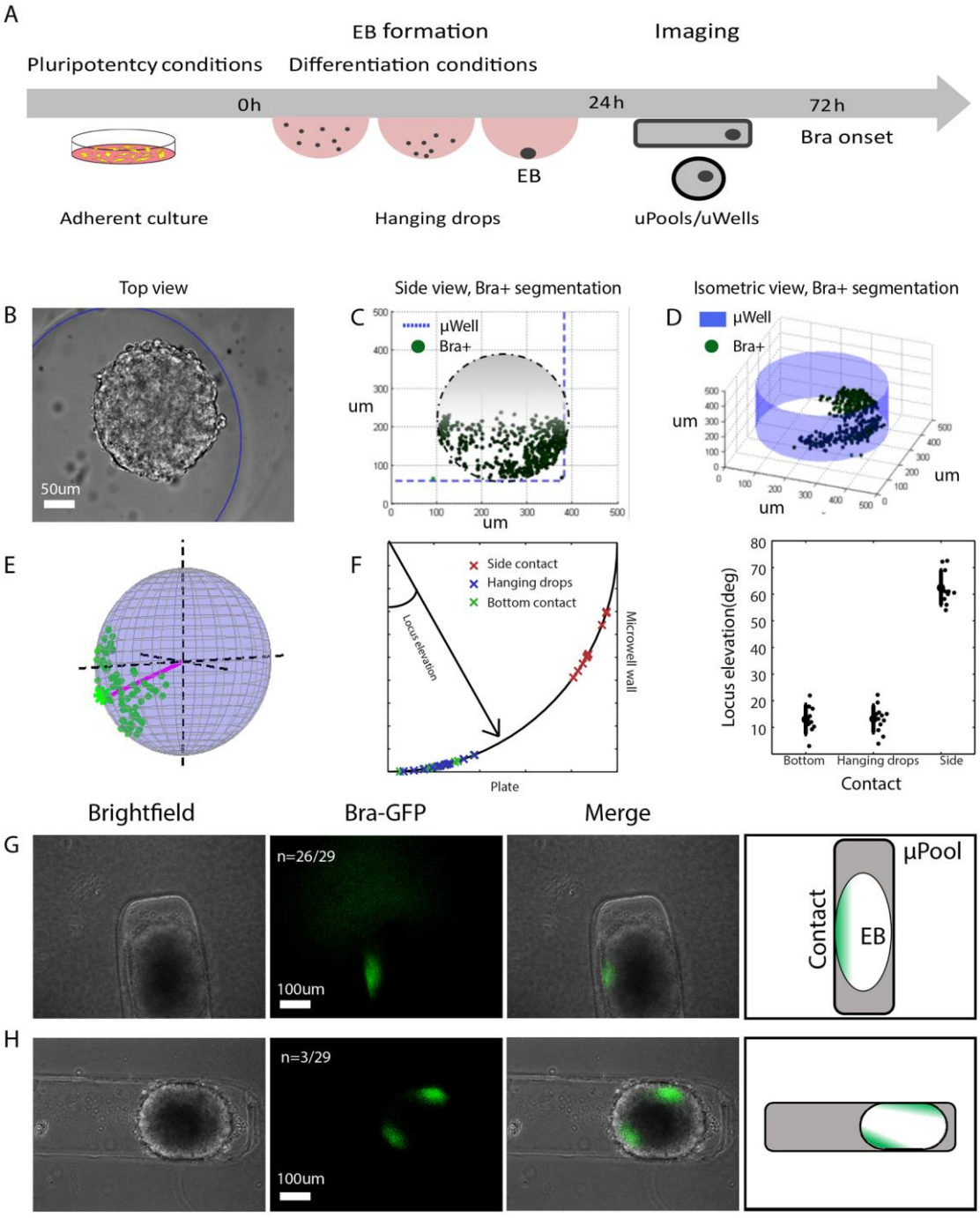


**Fig 1. Bra activation is influenced by contact.** (A) Description of the micro wells/pools experiment flow. (B) An EB in a microwell at 72 hrs from aggregation. Microwell walls are outlined with a blue circle. (C) Segmented Bra signal for the EB from panel A, at sagittal view aspect, showing Bra onset from the contact. (D) An EB touching the well walls at two points.

Bra onsets from both points. (E) Estimating the spatial location of Bra locus on segmentation data. The locus vector is shown in magenta. The blue sphere denotes the full EB volume. (F) Locus elevation angle for EBs with bottom contact only (green marks) or side contact (red marks) as determined from the brightfield channel at t = 60 hrs, as well as for EBs differentiated and imaged in hanging drops at t = 72 hrs (blue marks). The EBs are depicted on a quarter circle (left) or as mean with stdev error bars (right). Locus elevation is largely determined by contact point. For bottom onset, the locus angle is biased upwards due to asymmetric expansion of Bra+ cells in azimuth. For side onset, the locus angle is biased downwards due to a positive slope of the microwell walls. EBs with dual side and bottom locus were omitted from the analysis for visualization clarity. (G-H) Enforcing contact points by growing EBs in narrow micropools (200 um wide) affects Bra locus locations (see text): (G) Single side locus example, (H) Double side loci example.

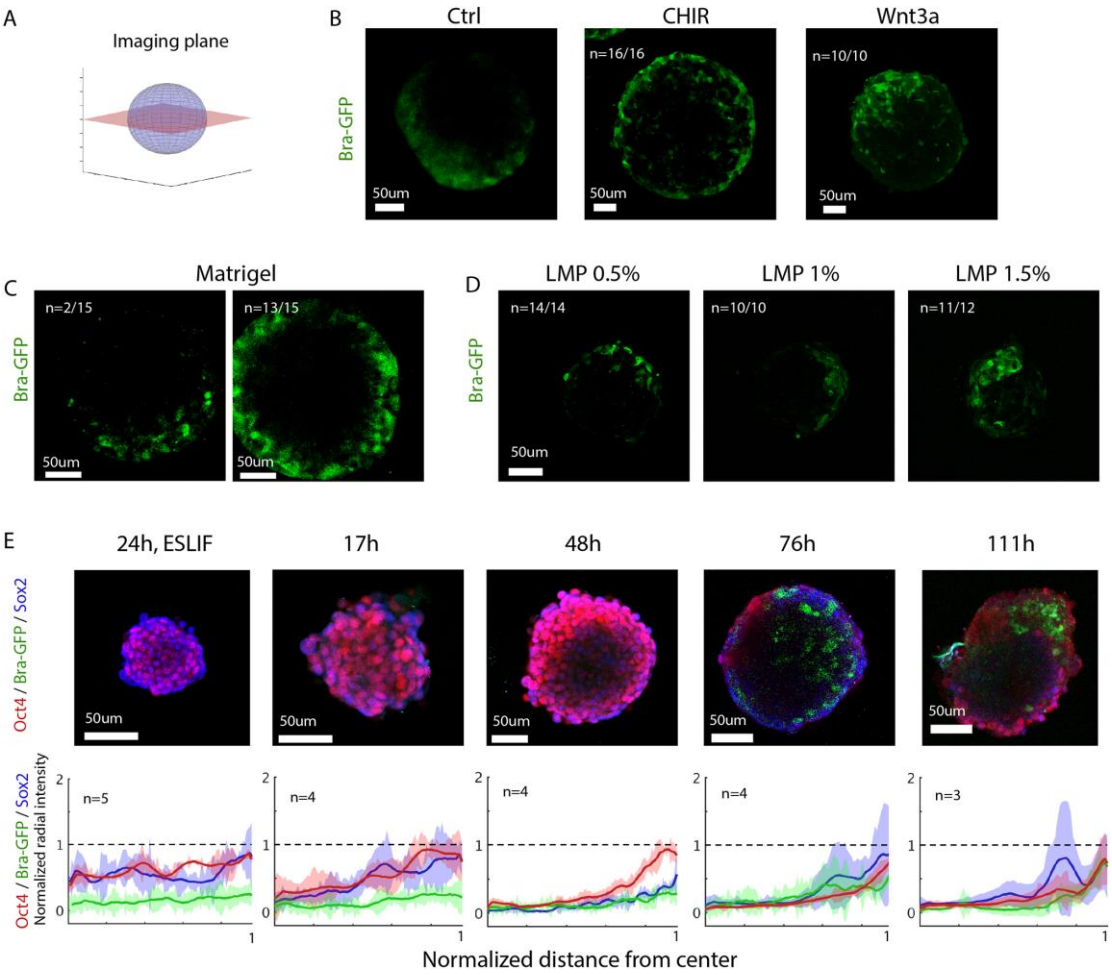


**Fig 2. A Bra competent layer is formed prior to onset on the outer shell of the EB.** (A) EBs are imaged at the equatorial slice. (B) Treatment with CHIR between 0-72 hrs (middle) triggers Bra onset on the entire shell, compared to control (left), or soluble Wnt3a treatment (right), which show a polarized onset. (C) Embedding EBs in Matrigel leads to Bra onset isotropically in most (13/15) EBs (right), or from a single locus in some (2/15) large EBs (left). (D) Embedding EBs in low melting point agarose with various concentrations had no effect on Bra locus. (E) Immunostaining of Sox2 and Oct4 in E14 Bra-GFP EBs at the indicated time points after aggregation. Top row: equatorial slices. Bottom row: normalized radial intensity profiles of Oct4, Bra and Sox2, computed in the direction of maximal expression on the outer shell, averaged over the indicated number of EBs. Shaded area marks standard deviation.

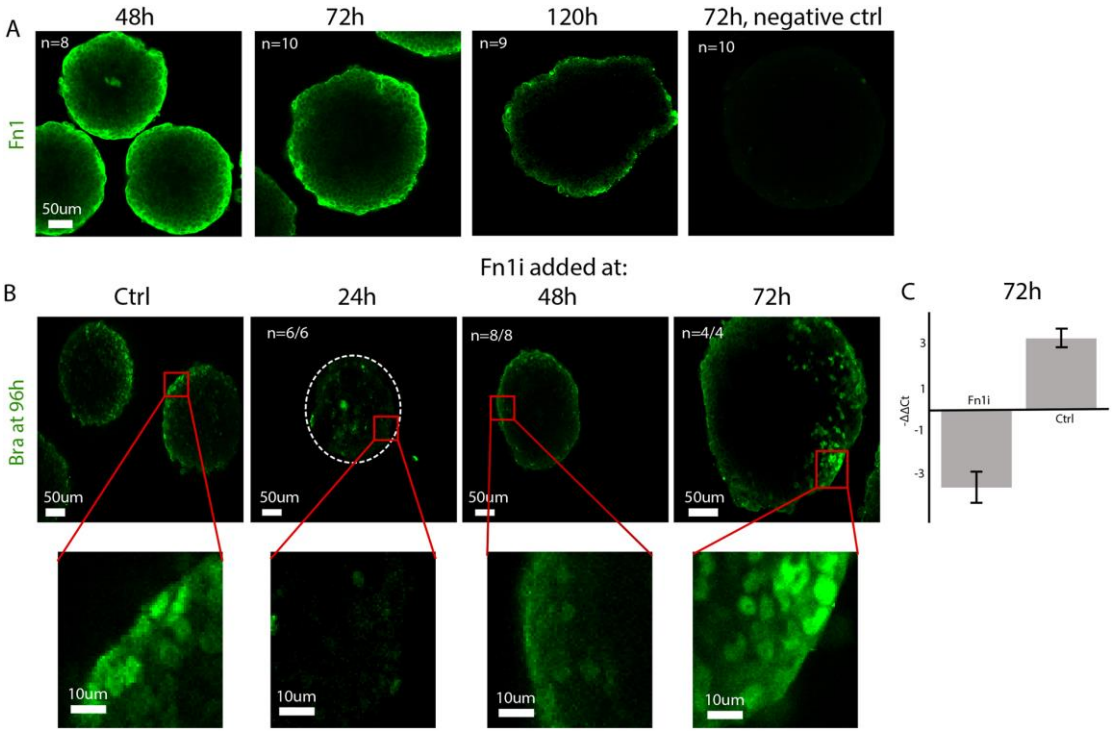


**Fig 3. Fibronectin is expressed isotropically on the EB outer shell, and is needed at early stages for Bra expression.** (A) Fibronectin immunostaining at 48, 72 and 96hrs/120hrs from aggregation in R1 derived EBs. Fibronectin is expressed uniformly on the outer shell at early stages, however it declines by 120 hrs. Negative control (right) shows secondary-only staining. Shown example for each condition is representative of all imaged EBs. (B) EBs subjected to fibronectin inhibition by an anti-Fn1 antibody starting at 24, 48 or 72 hrs from aggregation, and immunostained for Bra (green) at 96 hrs (close to the onset time in R1 derived EBs). Fibronectin inhibition prevents Bra onset, but only when started earlier than 48 hours. (C) Bra levels measured by RT-PCR, showing Bra expression fold change between control group (no treatment) and Fn1i treatment group. Fn1i was added at aggregation. Mean and standard deviation over 3 primer pairs and 2 replicates each are shown (P<1e-4, see Methods).

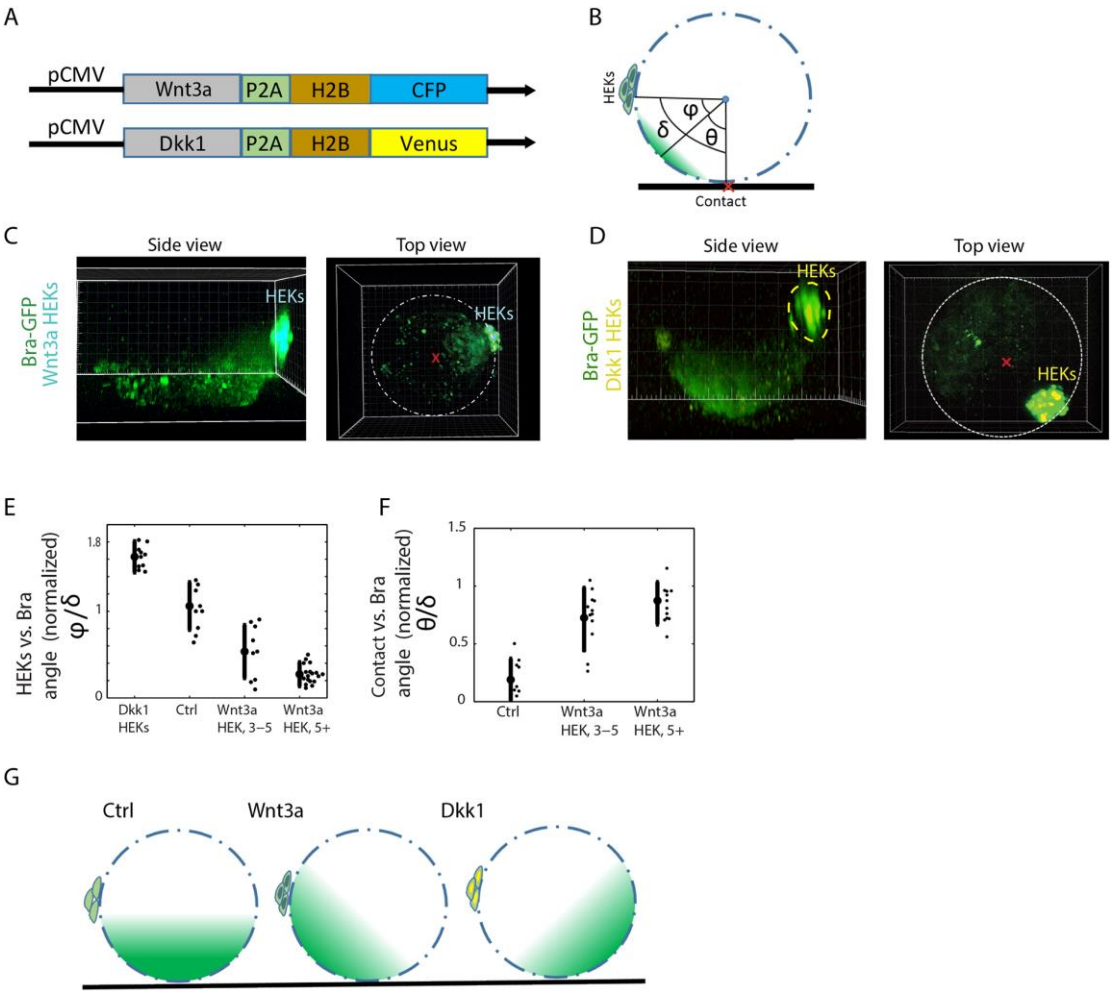


**Fig 4. Bra onset locus is determined by contact and Wnt signaling integration.** (A) Wnt3a and Dkk1 constructs used for ligand secretion from HEK cells. (B) A signal source (a clump of transfected HEK cells) is embedded into each EB. After 72 hrs of differentiation, the position of the signal source and the Bra locus are determined, as in Fig. 1D. The pairwise spatial angles between signal source, contact point with well bottom surface (red x mark) and Bra locus are then computed. (C) Example of an EB with a Wnt3a signaling source. Bra onset locus is biased towards the Wnt3a secreting HEKs. (D) Example of an EB with a Dkk1 signaling source. Bra onset locus is biased away from the Dkk1 secreting HEKs. (E) Angle between HEK signaling source and Bra locus ($\varphi$) normalized by the angle between the HEKs and the contact point ($\delta$). Wnt3a secretion biases onset from the contact point towards the Wnt source in a quantity dependent manner, where Dkk1 secretion biases the locus away to the opposite side. $P<0.05$ for all group pairs, two-sample KS test. (F) Angle between contact point and Bra locus ($\theta$) normalized by the angle between the HEKs and the contact point ($\delta$). (G) A schematic description of the spatial bias effect.

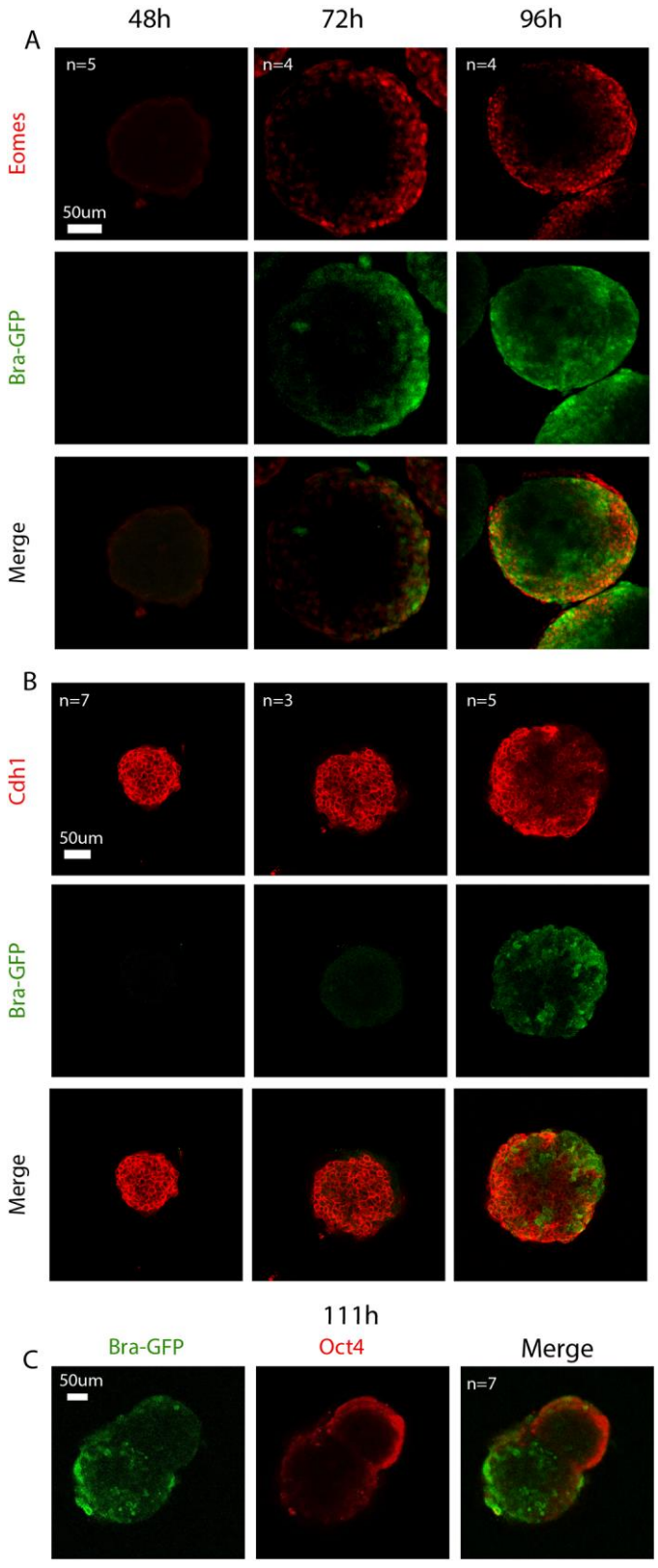

**Fig 5. Brachyury onsets in a primitive streak like area in EBs.** Immunostaining of early developmental markers, comparing their spatial expression patterns to that of Brachyury. (A) Eomes onsets with Bra at the same locus and extends beyond Bra spatial expression. (B) E-cadherin recedes from the locus where Bra appears, allowing cell motility. (C) Oct4 is expressed on the outer shell, then receding to the pole opposite that of Bra onset. Shown example for each condition is representative of all imaged EBs under that condition.

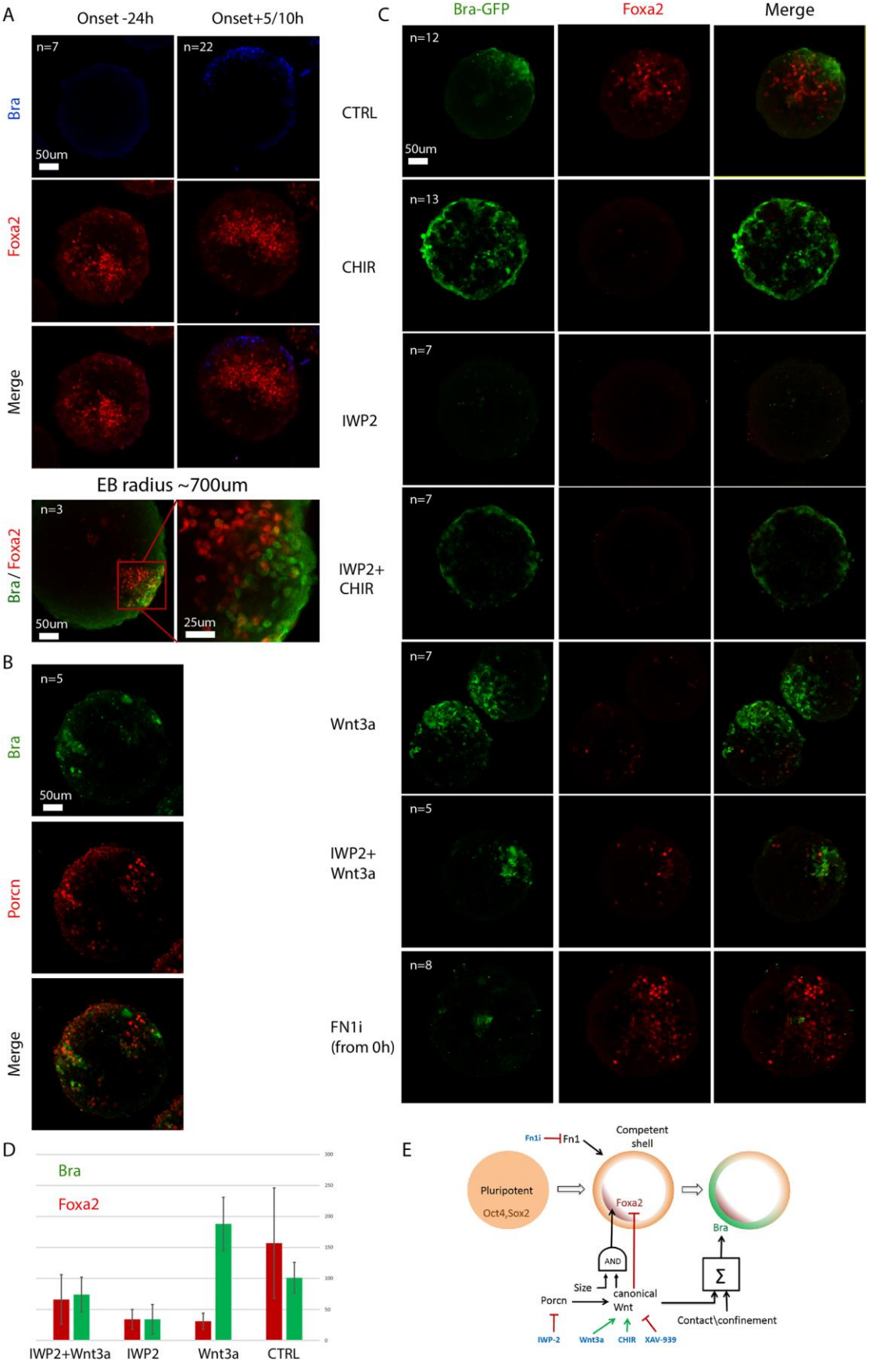

**Fig 6. Foxa2 is a Wnt dependent precursor to symmetry breaking and Bra expression locus.** (A) Foxa2 expression is juxtaposed to Bra+ cells in EBs, appearing >24 hrs before the onset of Bra (n>20, multiple experiments). Bottom: Foxa2/Bra pattern in a large (700um) EB (similar pattern seen in 3/3 large EBs). (B) Porcn expression partially overlaps with Bra, suggesting that Wnt ligands can be secreted in these cells. (C) CHIR upregulates Bra, triggers an isotropic expression pattern on the Bra-competent outer shell while downregulating Foxa2 expression in the EB; IWP2 (a porcupine inhibitor) inhibits Wnt secretion, downregulating Foxa2 and Bra; CHIR rescues Bra under IWP2 perturbation, however Foxa2 is still downregulated; Wnt3a up regulates Bra while down regulating Foxa2; Wnt3a partially rescues both Bra and Foxa2 under IWP2; Fn1 inhibition abolishes Bra expression but leaves Foxa2 intact. All signals were applied from 48 hrs after aggregation, except Fn1 inhibition, applied at 0 hrs. Patterns are representative for all imaged EBs in each condition. (D) Perturbation effects on Bra and Foxa2 expression quantified as number of highly expressing cells per EB. (E) A schematic model summarizing the factors affecting Foxa2 and Bra onset in the EB.

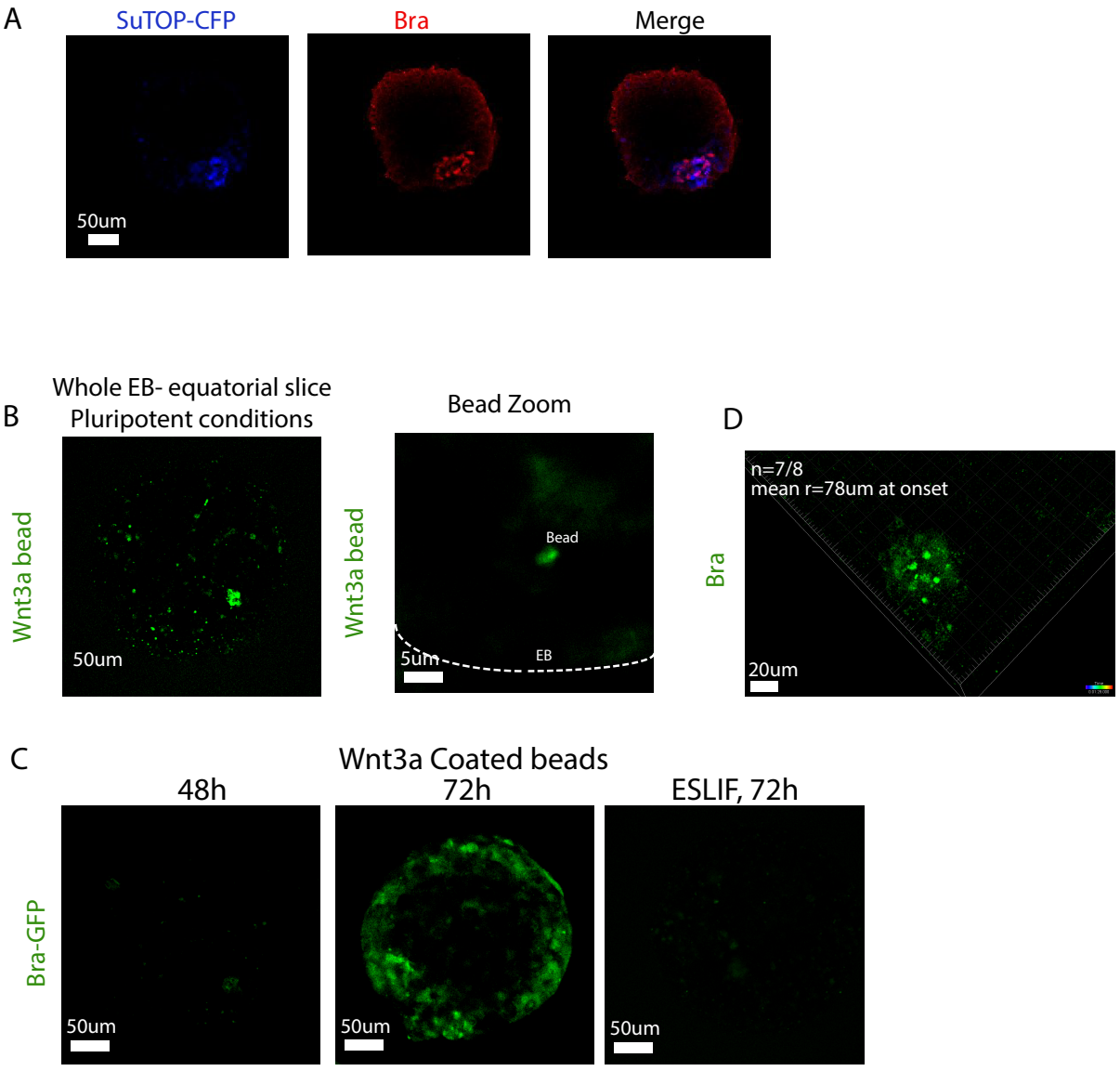


**Fig S1. Wnt3a beads integration and small-EB isotropic onset.** (A) Bra co-localizes with canonical Wnt response in SuTOP-CFP cells. (B) Left: An equatorial slice of an EB embedded with multiple Wnt3a-coated beads (green). Right: A zoom in snapshot on a Wnt3a-coated bead. (C) Wnt3a-coated embedded beads have no effect on Bra onset in pluripotent conditions (right) or in early differentiation (left), however onset is isotropical on the shell at 72 hrs. (D) An example small EB differentiated in microwells at 72 hrs from aggregation, showing isotropic (spatially uniform) Bra expression onset. The isotropic pattern occurred in 7/8 small EBs (radius at onset = 78+-10um)

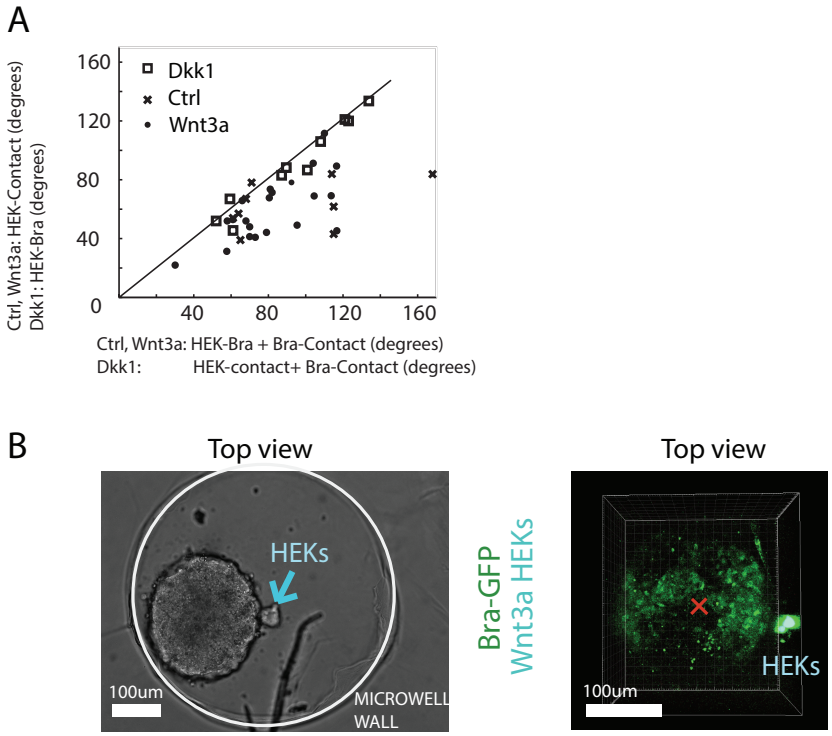


**Fig S2. Wnt3a/Dkk1 source, Bra locus, and contact point show high co-planarity.** (A) The angle between HEKs signal source and contact ($\delta$, Y-axis) vs. the sum of the angle between HEKs to Bra locus and the angle between Bra locus and contact ($\theta+\varphi$, X-axis) for all EBs quantified in Fig. 4E,F. For EBs harboring Dkk1 or Wnt3a producing HEKs, $\delta$ is approximately equal to $\theta+\varphi$, indicating that Bra locus inhabits the same plane defined by the HEKs, contact point and the EB centroid. As expected, in control EBs there is a larger deviation from co-planarity, as the Bra locus is not constrained to that same plane. (B) An example of double Bra loci, one triggered by localized Wnt signaling and the other from contact with the microwell wall.

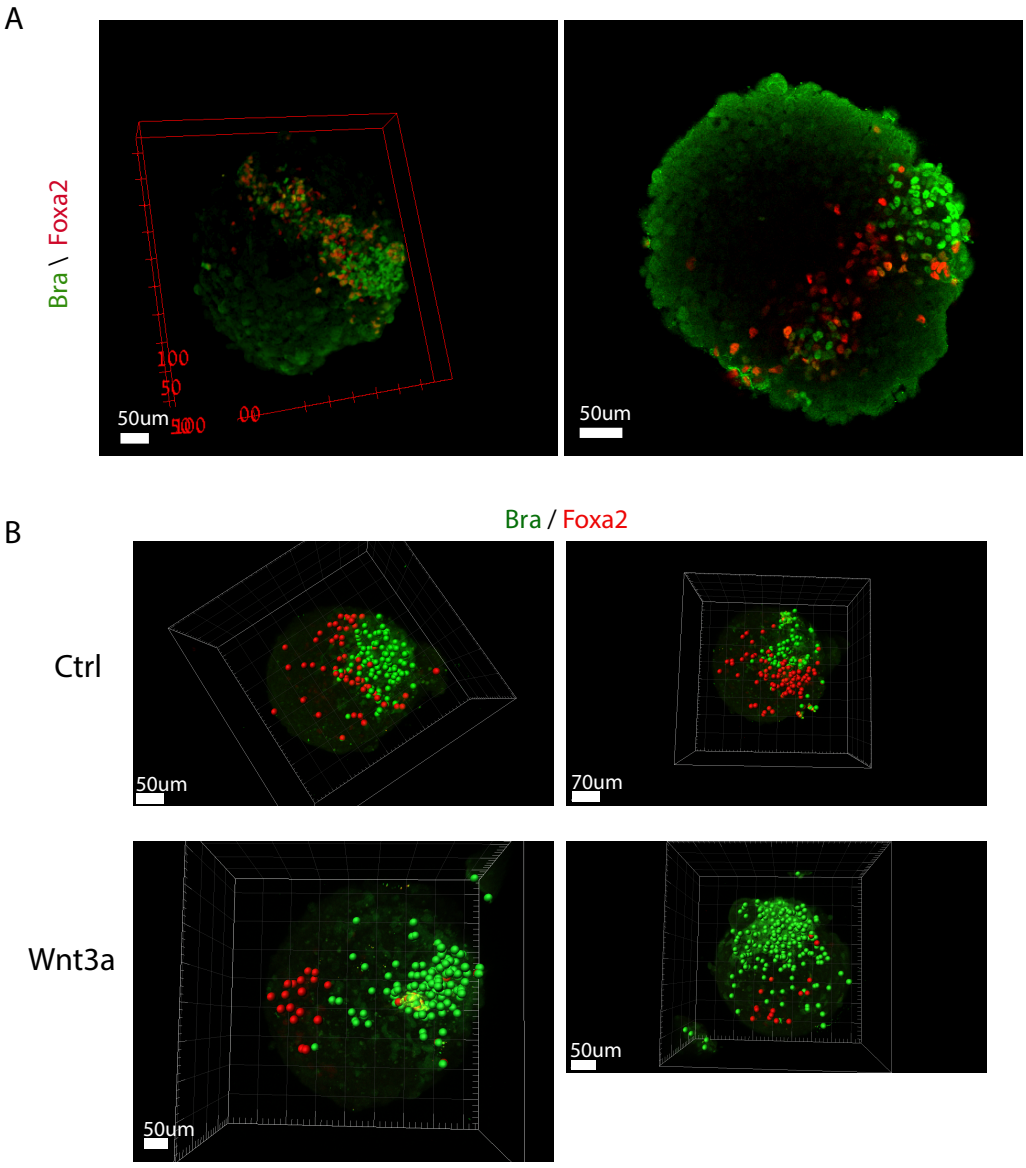


**Fig S3. Bra and Foxa2 are spatially adjacent in EBs but can be decoupled by external Wnt signaling.** (A) Immunostaining of Foxa2 and Bra at 72 hrs from aggregation. Foxa2 spatially correlates with Bra expression. (B) Segmentation of immunostained Foxa2 (red) and Bra (green) expressing cells at 72 hrs from aggregation. Foxa2 is adjacent to Bra locus in wild type EBs, while Wnt3a treated EBs show Foxa2 downregulation and spatial decoupling from Bra.

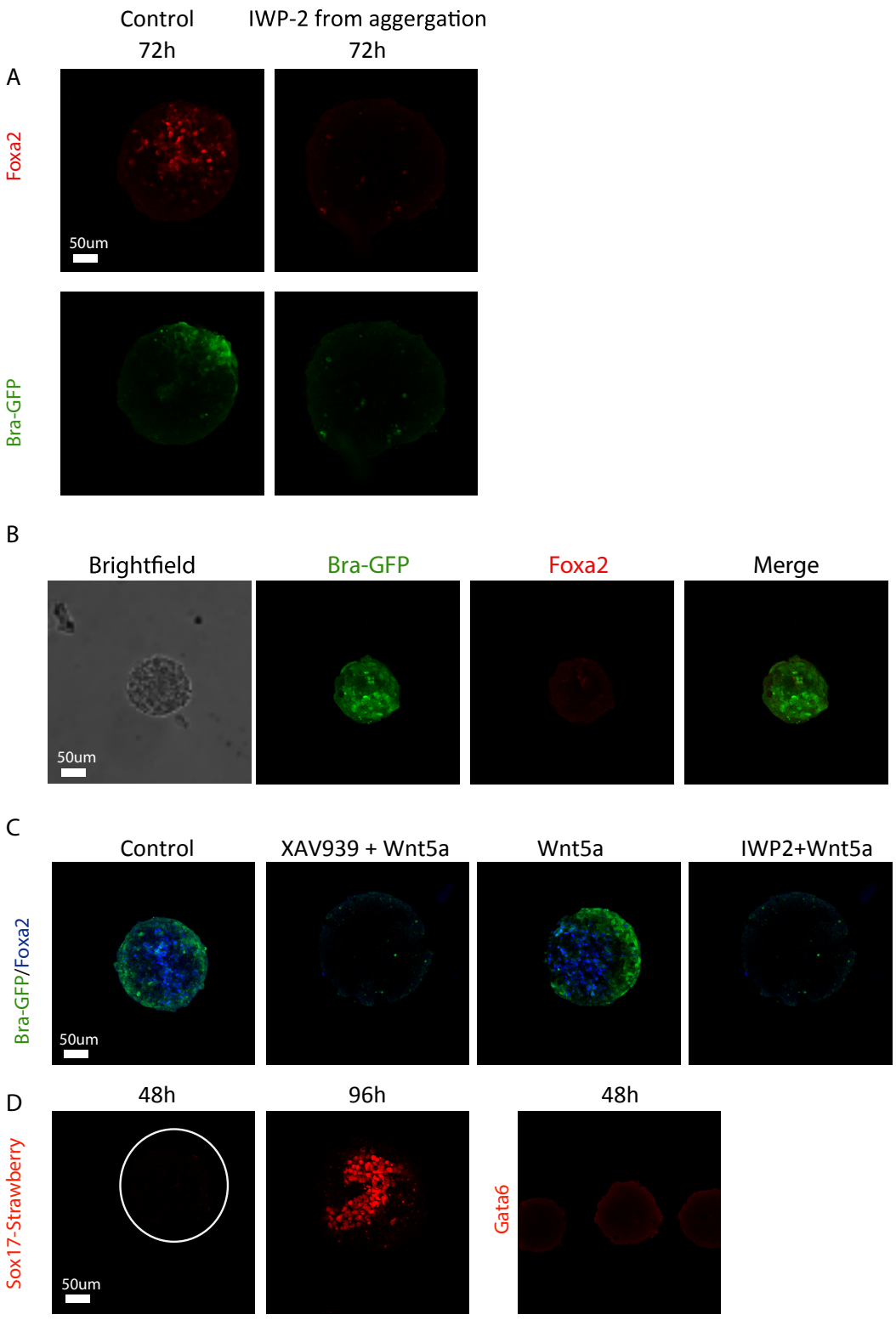


**Fig S4. Foxa2 expression abolished under IWP-2 treatment or in small sized EBs.** (A) Bra and Foxa2 are not expressed at 72 hrs under IWP-2 perturbation starting at 0 hrs from aggregation. (B) Small size EBs do not express Foxa2 at 72 hrs. (C) Foxa2 and Bra are not expressed under canonical Wnt inhibition (XAV939) or general Wnt inhibition (IWP2), and are not rescued by non-canonical Wnt activation (Wnt5a). (D) Sox17 and Gata6 are not expressed before Bra onset, indicating Foxa2+ cells at 48 hrs do not represent an endodermal lineage.

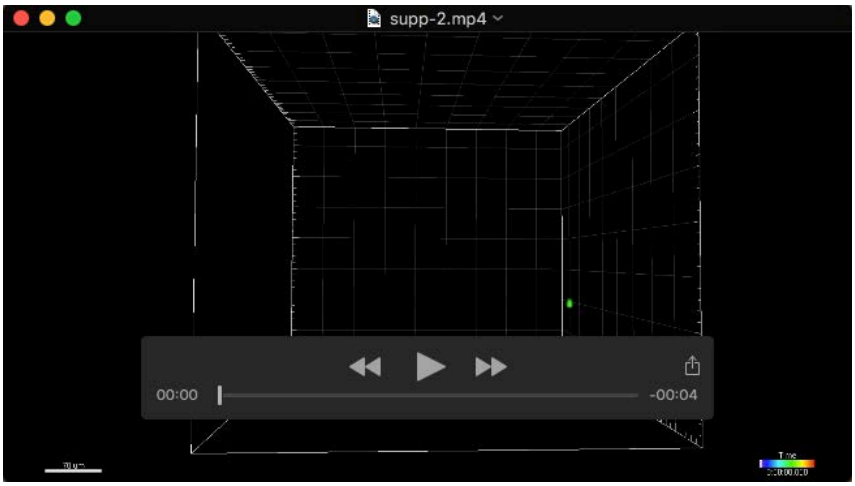


**Movie 1** Three-dimensional time-lapse imaging of Bra-GFP in two E14 Bra-GFP embryoid bodies, imaged in microwells between 60 and 96 hrs from aggregation and transfer to differentiation medium. Bra-GFP expression onsets at the bottom (contact point with the glass) , and expands upwards on the outer shell.

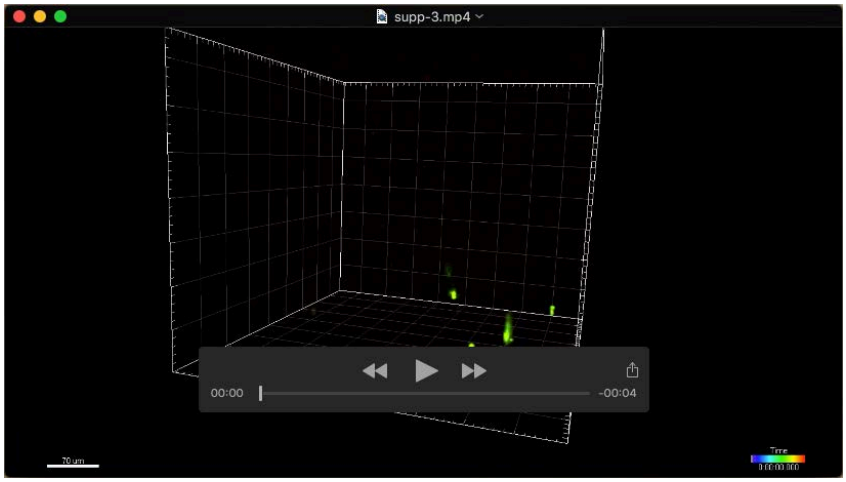


**Movie 2** Three-dimensional time-lapse imaging of Bra-GFP in two E14 Bra-GFP embryoid bodies, imaged in microwells between 60 and 96 hrs from aggregation and transfer to differentiation medium. Bra-GFP expression onsets at the bottom (contact point with the glass) , and expands upwards on the outer shell.

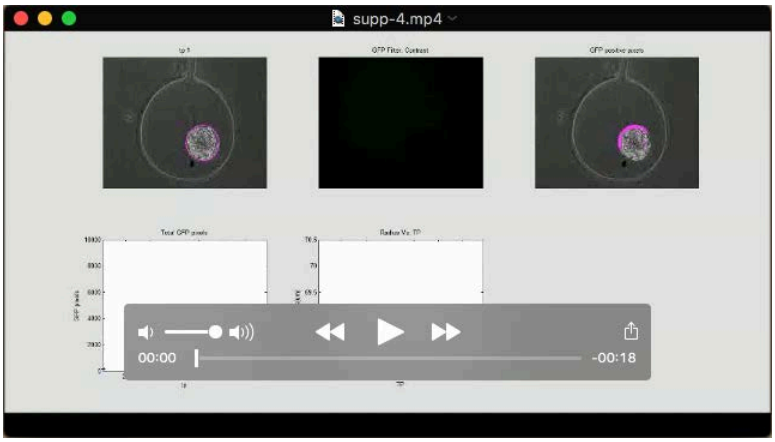


**Movie 3** Epifluorescence time-lapse of a Bra-GFP embryoid body, where Bra onset occurred at the bottom. The EB is imaged between 24 and 90 hrs from aggregation, where at 24 hrs it was transferred to a microwell. Top row: left - brightfield imaging of the EB with its encompassing perimeter; center - Bra-GFP; right – overlay of brightfield and GFP-positive pixels (magenta) . Bottom row: left - total Bra-GFP+ pixels vs. time point (time interval between points – 30 minutes) . Blue line - raw data; red dashed line: alpha filter smoothing; yellow line: Bra onset threshold defined as 500 GFP+ pixels; center – EB radius vs. timepoint. Noise at higher time points is due to manual estimation of radius; right – snapshot of Bra-GFP onset frame.

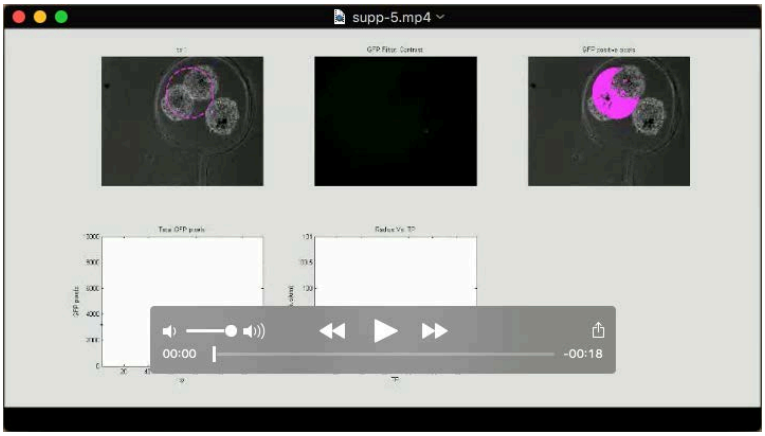


**Movie 4** Similar to Movie S3, for a case where Bra expression onset occurred at the contact point with the microwell side. Note in this case the EB originated from 3 smaller EBs that merged together after transfer to the microwell.

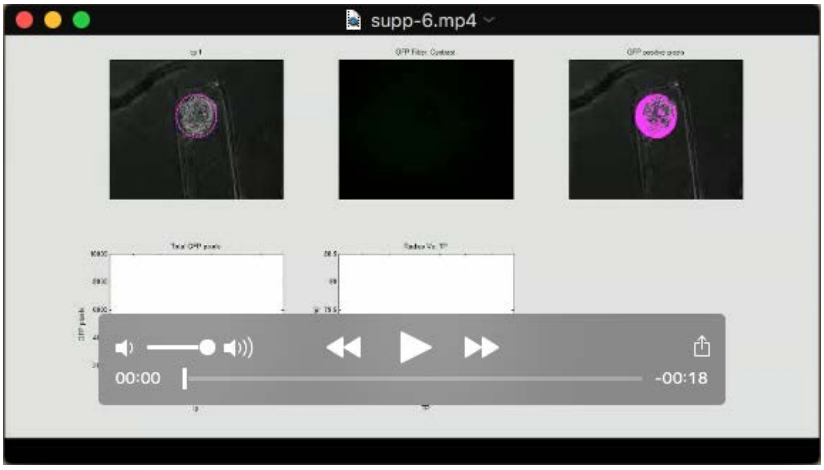


**Movie 5** Similar to Movie S3, for an EB differentiated in an elongated micropool (width=200um). In this case, Bra-GFP expression onsets from two different loci (around t.p. 121), at the two sides compressed against the well walls. At t.p. 130 the EB pops out of the channel, resulting in a change in its focus.


**Movie 6** Similar to Movie S5, for a case where Bra expression onsets from one of the compressed sides of the EB.

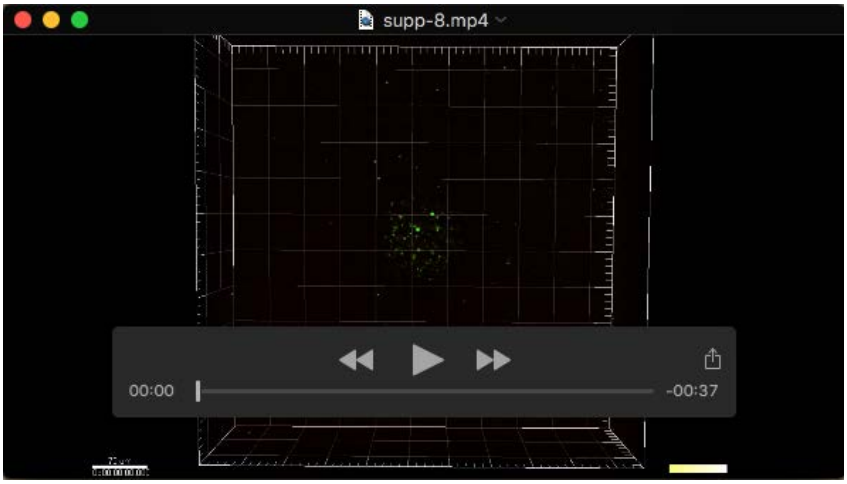


**Movie 7** Time lapse of an EB differentiated while embedded in Matrigel. Bra onset occurs uniformly from the whole sphere, representative of the dynamics in 13/15 imaged EBs.

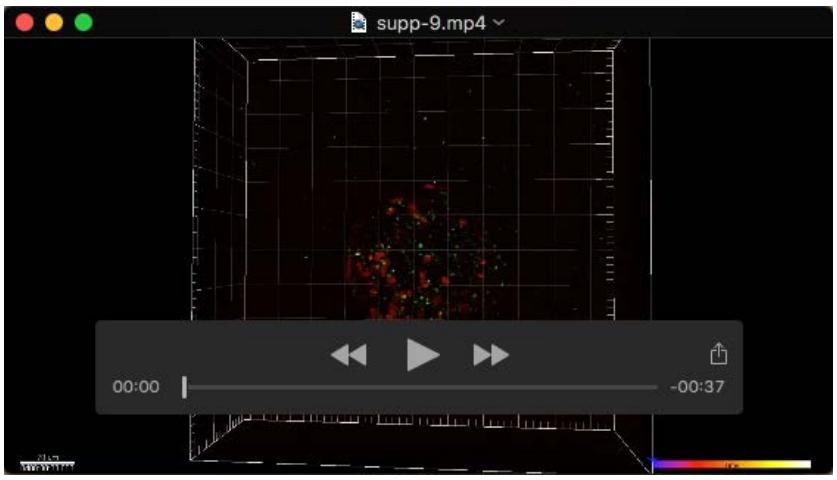


**Movie 8** A Bra-GFP, pCMV-Strawberry large EB differentiated while embedded in Matrigel. Bra expression onsets from one locus, expanding from that point into the whole sphere. This dynamic represents 2/15 imaged EBs.

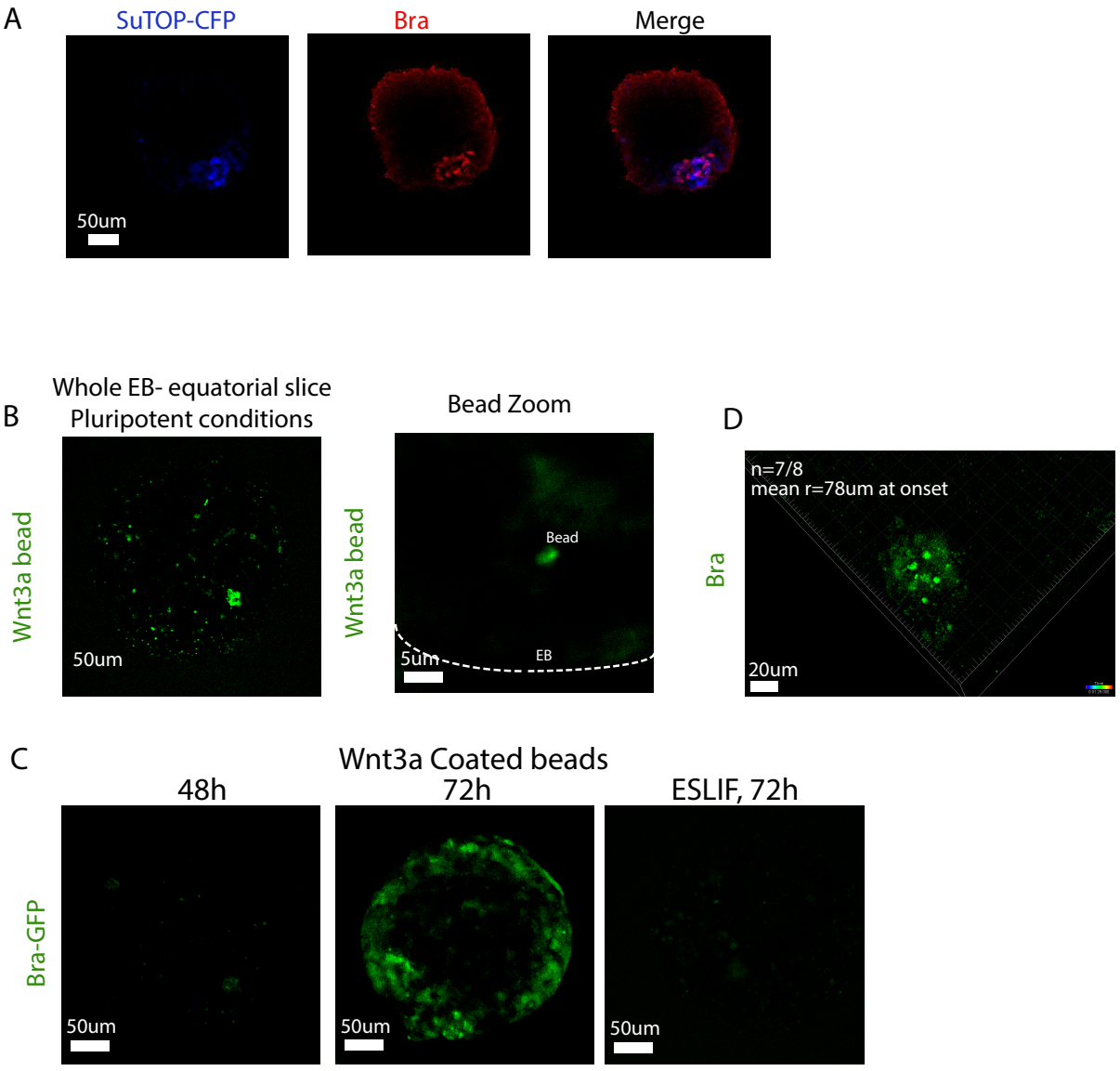


**Fig S1. Wnt3a beads integration and small-EB isotropic onset.** (A) Bra co-localizes with canonical Wnt response in SuTOP-CFP cells. (B) Left: An equatorial slice of an EB embedded with multiple Wnt3a-coated beads (green). Right: A zoom in snapshot on a Wnt3a-coated bead. (C) Wnt3a-coated embedded beads have no effect on Bra onset in pluripotent conditions (right) or in early differentiation (left), however onset is isotropical on the shell at 72 hrs. (D) An example small EB differentiated in microwells at 72 hrs from aggregation, showing isotropic (spatially uniform) Bra expression onset. The isotropic pattern occurred in 7/8 small EBs (radius at onset = 78+-10um)

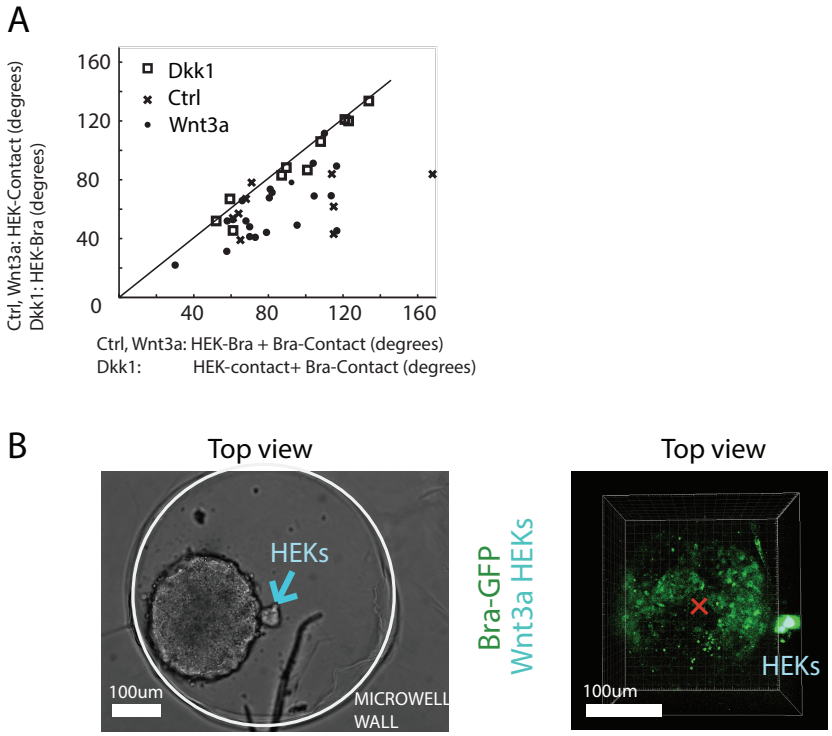


**Fig S2. Wnt3a/Dkk1 source, Bra locus, and contact point show high co-planarity.** (A) The angle between HEKs signal source and contact ($\delta$, Y-axis) vs. the sum of the angle between HEKs to Bra locus and the angle between Bra locus and contact ($\theta+\varphi$, X-axis) for all EBs quantified in Fig. 4E,F. For EBs harboring Dkk1 or Wnt3a producing HEKs, $\delta$ is approximately equal to $\theta+\varphi$, indicating that Bra locus inhabits the same plane defined by the HEKs, contact point and the EB centroid. As expected, in control EBs there is a larger deviation from co-planarity, as the Bra locus is not constrained to that same plane. (B) An example of double Bra loci, one triggered by localized Wnt signaling and the other from contact with the microwell wall.

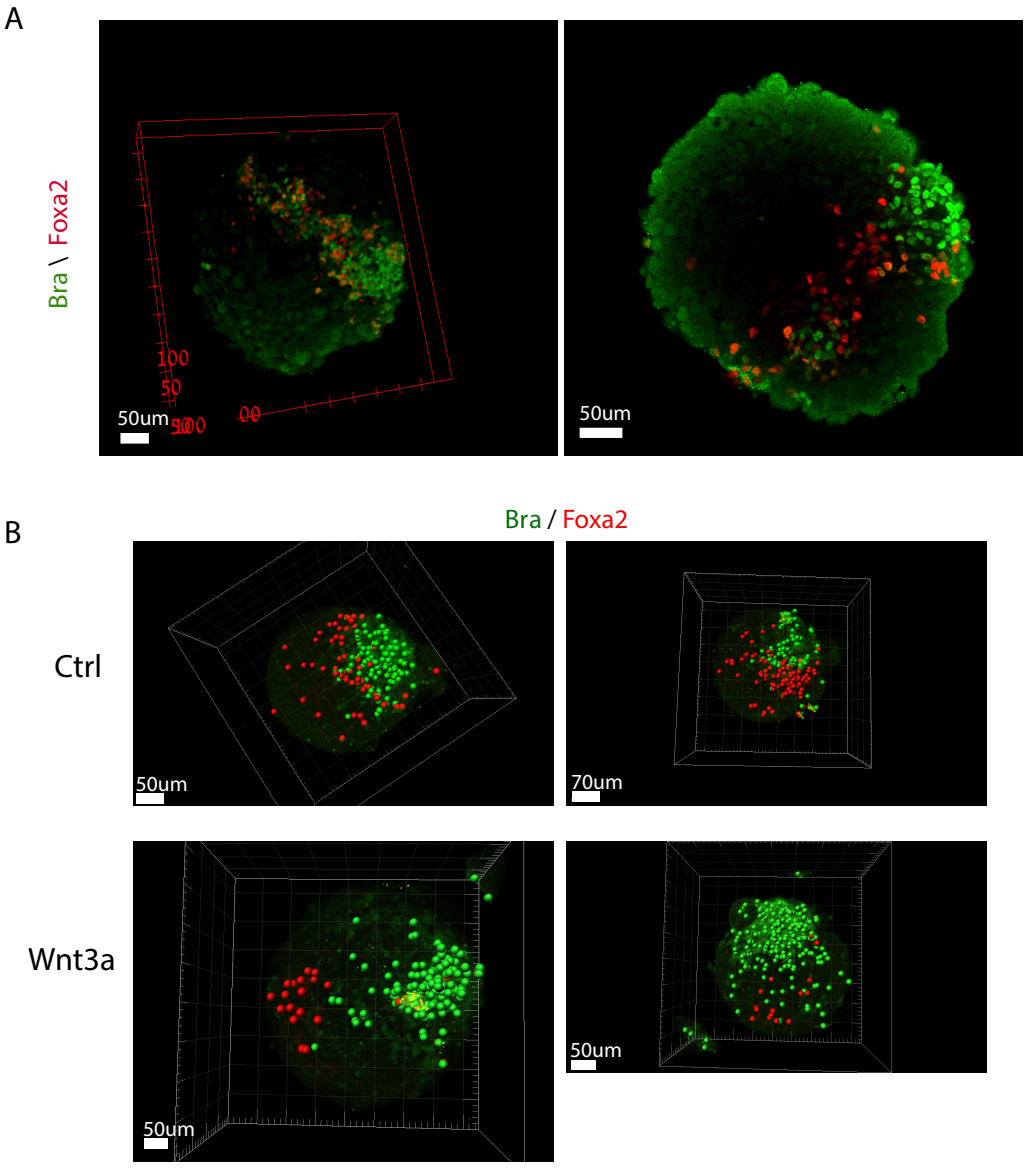


**Fig S3. Bra and Foxa2 are spatially adjacent in EBs but can be decoupled by external Wnt signaling.** (A) Immunostaining of Foxa2 and Bra at 72 hrs from aggregation. Foxa2 spatially correlates with Bra expression. (B) Segmentation of immunostained Foxa2 (red) and Bra (green) expressing cells at 72 hrs from aggregation. Foxa2 is adjacent to Bra locus in wild type EBs, while Wnt3a treated EBs show Foxa2 downregulation and spatial decoupling from Bra.

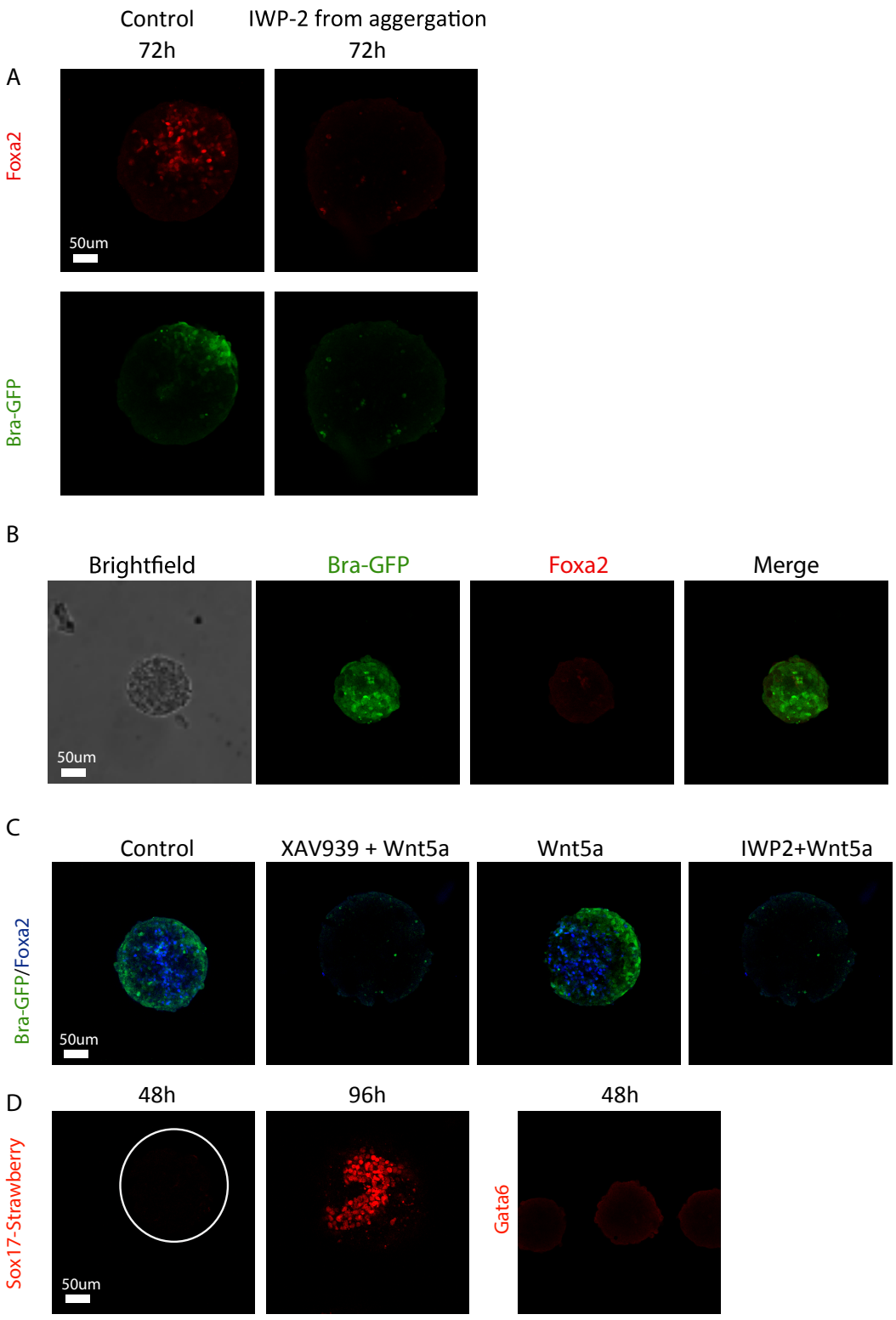


**Fig S4. Foxa2 expression abolished under IWP-2 treatment or in small sized EBs.** (A) Bra and Foxa2 are not expressed at 72 hrs under IWP-2 perturbation starting at 0 hrs from aggregation. (B) Small size EBs do not express Foxa2 at 72 hrs. (C) Foxa2 and Bra are not expressed under canonical Wnt inhibition (XAV939) or general Wnt inhibition (IWP2), and are not rescued by non-canonical Wnt activation (Wnt5a). (D) Sox17 and Gata6 are not expressed before Bra onset, indicating Foxa2+ cells at 48 hrs do not represent an endodermal lineage.

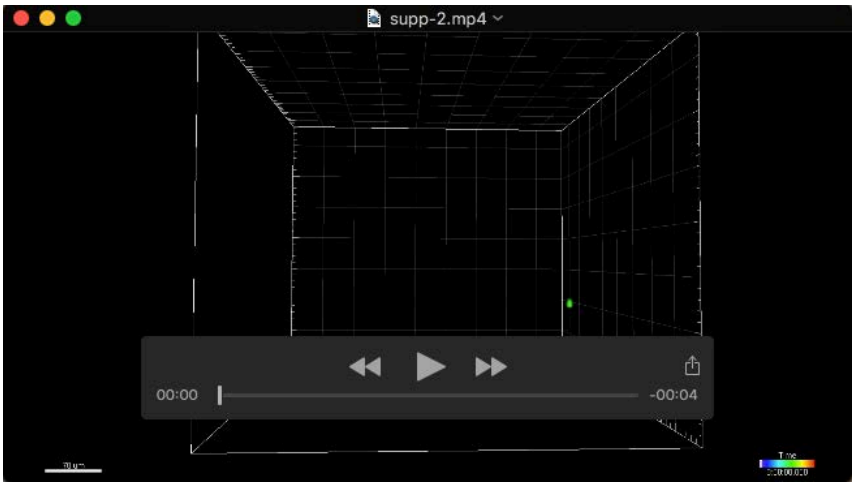


**Movie 1** Three-dimensional time-lapse imaging of Bra-GFP in two E14 Bra-GFP embryoid bodies, imaged in microwells between 60 and 96 hrs from aggregation and transfer to differentiation medium. Bra-GFP expression onsets at the bottom (contact point with the glass) , and expands upwards on the outer shell.

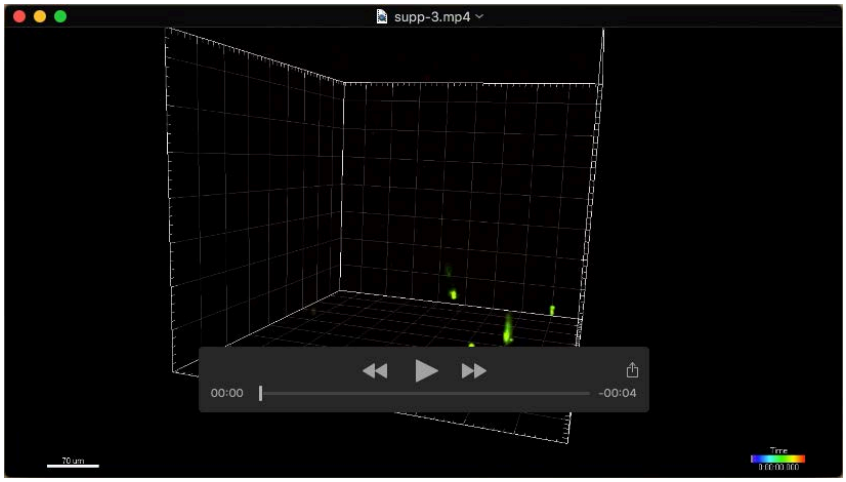


**Movie 2** Three-dimensional time-lapse imaging of Bra-GFP in two E14 Bra-GFP embryoid bodies, imaged in microwells between 60 and 96 hrs from aggregation and transfer to differentiation medium. Bra-GFP expression onsets at the bottom (contact point with the glass) , and expands upwards on the outer shell.

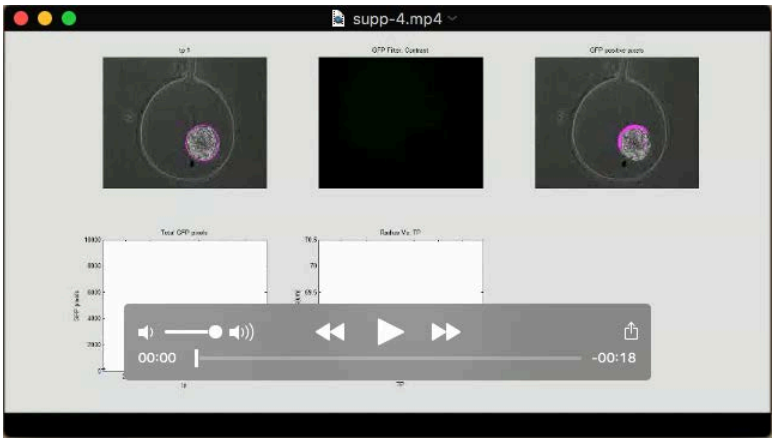


**Movie 3** Epifluorescence time-lapse of a Bra-GFP embryoid body, where Bra onset occurred at the bottom. The EB is imaged between 24 and 90 hrs from aggregation, where at 24 hrs it was transferred to a microwell. Top row: left - brightfield imaging of the EB with its encompassing perimeter; center - Bra-GFP; right – overlay of brightfield and GFP-positive pixels (magenta) . Bottom row: left - total Bra-GFP+ pixels vs. time point (time interval between points – 30 minutes) . Blue line - raw data; red dashed line: alpha filter smoothing; yellow line: Bra onset threshold defined as 500 GFP+ pixels; center – EB radius vs. timepoint. Noise at higher time points is due to manual estimation of radius; right – snapshot of Bra-GFP onset frame.

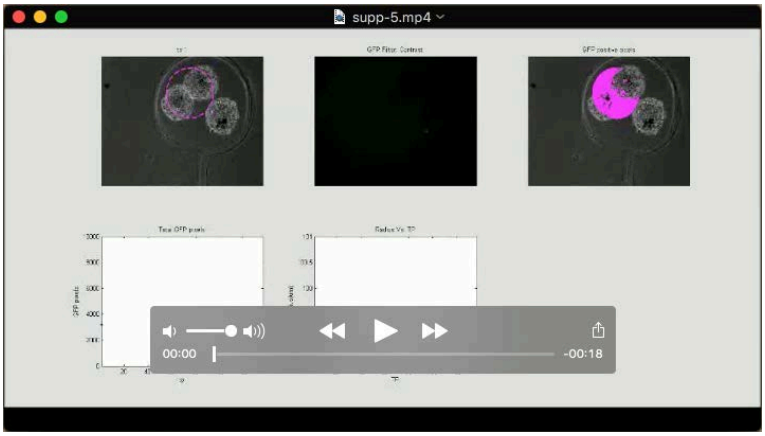


**Movie 4** Similar to Movie S3, for a case where Bra expression onset occurred at the contact point with the microwell side. Note in this case the EB originated from 3 smaller EBs that merged together after transfer to the microwell.

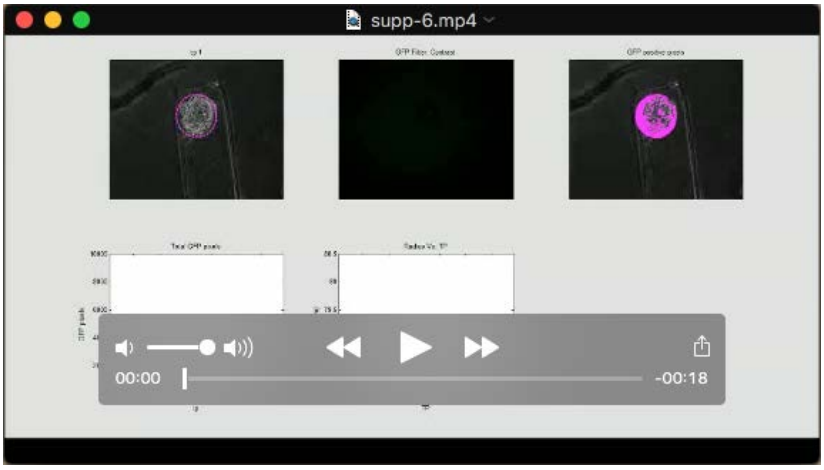


**Movie 5** Similar to Movie S3, for an EB differentiated in an elongated micropool (width=200um). In this case, Bra-GFP expression onsets from two different loci (around t.p. 121), at the two sides compressed against the well walls. At t.p. 130 the EB pops out of the channel, resulting in a change in its focus.


**Movie 6** Similar to Movie S5, for a case where Bra expression onsets from one of the compressed sides of the EB.

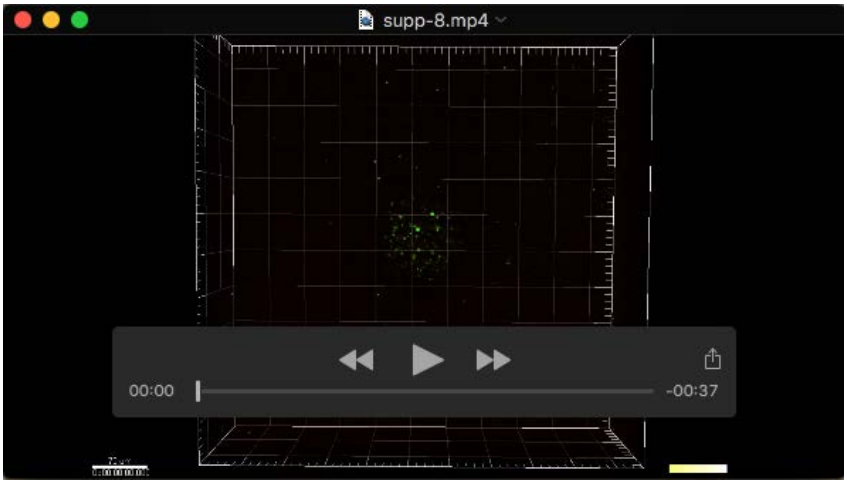


**Movie 7** Time lapse of an EB differentiated while embedded in Matrigel. Bra onset occurs uniformly from the whole sphere, representative of the dynamics in 13/15 imaged EBs.

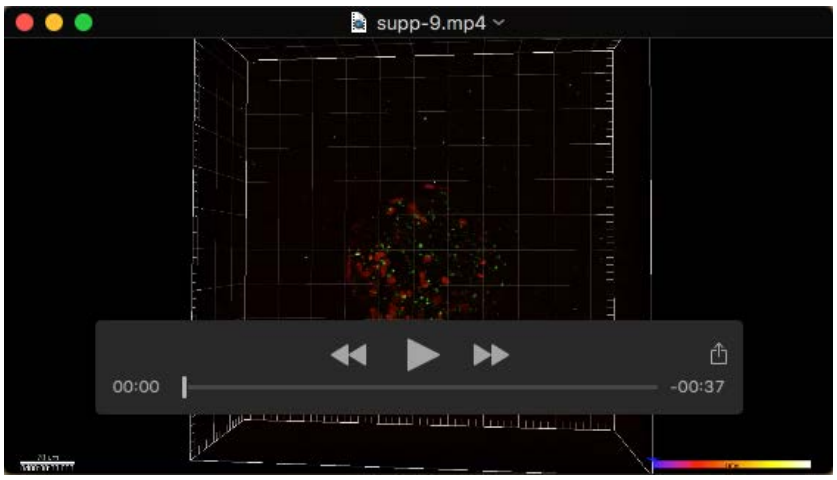


**Movie 8** A Bra-GFP, pCMV-Strawberry large EB differentiated while embedded in Matrigel. Bra expression onsets from one locus, expanding from that point into the whole sphere. This dynamic represents 2/15 imaged EBs.